FIBER OPTIC BASED CONTINUOUS WAVE FUNCTIONAL NEAR INFRARED SPECTROSCOPY SYSTEM

by

Barış Özkerim

B.Sc., in Electronics Engineering, F.M.V. Işık University, 2004

Submitted to the Institute of Biomedical Engineering
in partial fulfillment of the requirements
for the degree of
Master of Science
in
Biomedical Engineering

Boğaziçi University
January 2008

ACKNOWLEDGMENTS

I would like to thank my advisor Assist. Prof. Dr. Ata Akın for his endless support, encouragement and motivation throughout this work.

I would like to express my gratitudes to Prof. Dr. Mehmed Özkan and Assoc. Prof. Dr. Yasemin Kahya for being a member of my jury and for their invaluable comments and helpful discussions during the defense.

I am very grateful to Ömer Şaylı for his endless help in the theoritical considerations and in the experiments. I would also like to thank Filiz Ateş who gave me a whole day for the animal experiments.

I thank all the application engineers from IC Haus integrated circuits company and Thorlabs incorporation for their help in the design and implementation.

I thank Nermin Topaloğlu, Sinem Serap and Esin Karahan for their amicable friendship.

I am also grateful to Enver Atalı from Unimed Ltd. who gave me two months vacation to complete my thesis.

I am very grateful to Ercan Kara who made great contributions to every step of my work theoritically and practically. He took me to my home countless times at the nights after study. He helped me with his knowledge, ideas and especially with his friendship.

Finally, I would like to sincerely acknowledge the great support, encouragement and patience of my family throughout my studies.

ABSTRACT

FIBER OPTIC BASED CONTINUOUS WAVE FUNCTIONAL NEAR INFRARED SPECTROSCOPY SYSTEM

In the last decade, functional near-infrared spectroscopy (fNIRS) has been introduced as a new neuroimaging modality with which to conduct functional brain studies that require data collection from vision center or motor cortex. The main problem to get data from these regions is the presence of hair on the scalp. Furthermore, animal imaging requires miniaturized source and detectors to be placed on animal surface but there are no such components manufactured. Whereas, the use of fiber-coupled sources and detectors have allowed the investigation of cortical hemodynamics that lie underneath places covered with hair and also allowed the examination of the hemodynamic changes on the animal muscles.

The study is involved with driving and modulating two near infrared lasers as well as coupling the resulting coherent and collimated lights to the optical fibers via the optical converters. In addition, fiber optic cables with large core diameters are used to transmit the scattered light from the tissue to the photodetectors. The main goal of the study is to develop a portable and robust fNIRS system for the detection of cortical hemodynamic changes occurring during motor and visual tasks as well as for the study of animal hemodynamics.

The ability and effectiveness of the system is tested by several experiments based on the phantom, human and animal studies. Although the system can successfully operate up to one and a half centimeter source detector distance which is enough to examine the hemodynamic changes in the muscle and to work on the animal surface, it is not sufficient to examine the changes during the brain activity. This is mainly due to low signal to noise ratio (SNR) that can be increased with more powerful and fiber-pigtailed lasers.

Keywords: Near infrared spectroscopy, Optical imaging, Laser drivers.

ÖZET

FİBER OPTİK TABANLI SÜREKLİ DALGALI İŞLEVSEL YAKIN KIZIL ÖTESİ SPEKTROSKOPİ SİSTEMİ

İşlevsel yakın kızıl ötesi spektroskopi (iYKÖS) son yıllarda beyin çalışmalarında yeni bir sinir görüntüleme yöntemi olarak ortaya çıkmaktadır. Görüntüleme için görme merkezi ve motor korteks gibi saçla kaplı bölgelerden veri toplanması gerekliliği bu yöntemin en büyük problemlerinden biridir. Bunun dışında, hayvanlarda görüntüleme yapabilmek için küçük boyutlu kaynak ve detektörler gerekmektedir. Fakat, günümüzde yeteri kadar küçük kaynak ve detektörler üretilmemektedir. Oysa kaynakları ve dedektörleri fiber kabloya bağlanmış sistemler saçlı bölgelerin altındaki kortikal hemodinamikleri ve hayvanların kaslarındaki hemodinamikleri incelemeyi mümkün kılmaktadır.

Bu çalışmada iki adet yakın kızıl ötesi lazer sürülmüş ve modüle edilmiştir. Ortaya çıkan koherent ve hizalı lazer ışını fiberlere optik çeviricilerle bağlanmıştır. Bunun yanısıra, dokudan saçılan ışığı fotodedektörlere iletmek için geniş kor çaplı fiberler kullanılmıştır. Çalışmanın esas amacı motor ve görsel aktiviteler esnasında meydana gelen kortikal hemodinamik değişimleri ve hayvansal dinamikleri algılayabilmek için taşınabilir ve dayanıklı bir iYKÖS sistemi geliştirmektir.

Geliştirilen cihazın teknik özellikleri çeşitli fantom, insan ve hayvan deneyleri ile test edilmiştir. Sistem birbuçuk santimetre kaynak-dedektör mesafesine kadar düzgün bir şekilde çalışmaktadır. Bu kas üzerindeki hemodinamik değişimleri gözlemlemek için ve hayvansal görüntüleme yapmak için yeterli fakat beyinde meydana gelen değişimleri incelemek için yeterli değildir. Bunun başlıca sebebi sinyal gürültü oranının yeteri kadar büyük olmamasıdır. Bu, daha güçlü ve optik fiberi lazer ile bir imal edilmiş lazerler kullanılarak giderilebilir.

Anahtar Sözcükler: Yakın kızıl ötesi spektroskopi, Optik görüntüleme, Lazer sürücüleri.

TABLE OF CONTENTS

LIST OF FIGURES

LIST OF TABLES

LIST OF SYMBOLS

I	Transmitted light intensity
I_0	Incident light intensity
μ_a	Absorption coefficient
$1/\ \mu_a$	Absorption pathlength
T	Transmission
OD	Attenuation or optical density
c	Concentration
x	Thickness
ρ	Particle density
ε	Specific extinction coefficient
λ	Wavelength
L	Distance
B	Differential pathlength factor
G	Scattering losses
HbO_2	Oxyhemoglobin
Hb	Deoxyhemoglobin
Δ	Change
V	Voltage
A	Ampere
R	Resistor
v	Speed of light
t	Time
P_{nom}	Nominal power
P_{set}	Power to be set
ϕ	Phase shift
f	Frequency

LIST OF ABBREVIATIONS

fMRI	Functional Magnetic Resonance Imaging
PET	Positron Emission Tomography
fNIRS	Functional Near-Infrared Spectroscopy
EEG	Electroencephalography
LED	Light Emitting Diode
MBLL	Modified Beer-Lambert Law
APD	Avalanche Photodiode
PMT	Photomultiplier Tube
CCD	Charge Coupled Devices
MD	Monitor Diode
LD	Laser Diode
SMPS	Switch Mode Power Supply

1. INTRODUCTION

1.1 Motivation and Objective

Neuroimaging includes the use of various techniques to either directly or indirectly image the structure, function, or pharmacology of the brain. It is a relatively new discipline within medicine and neuroscience. It can be grouped into two broad categories as structural imaging and functional imaging. The former one deals with the overall structure of the brain and the precise diagnosis of intracranial disease and injury. The latter is used for neurological and cognitive science research and building brain-computer interfaces. It enables, for example, the processing of sensory information coming to the brain and of commands going from the brain to the organism to be "lit up" or visualized directly instead of by simple clinical inference [1].

Especially functional magnetic resonance imaging (fMRI) and positron emission tomography (PET) have been widely used during functional brain studies in humans. These techniques have greatly increased the knowledge about the neural circuits that underlie cognitive and emotional processes. However, these techniques are expensive, highly sensitive to motion artifact, confine the participants to restricted positions, and may expose individuals to potentially harmful materials (PET) or loud noises (fMRI). These characteristics make these imaging modalities unsuitable for many uses, including the monitoring of motor activity.

In the last decade, functional near-infrared spectroscopy (fNIRS) has been introduced as a new neuroimaging modality with which to conduct functional brain studies. fNIRS technology uses specific wavelengths of light (700nm – 900nm) , introduced at the scalp, to enable the noninvasive measurement of changes in the concentration of deoxygenated hemoglobin (deoxy-Hb) and oxygenated hemoglobin (oxy-Hb) during brain activity. This technology allows the design of portable, safe, affordable, non-invasive and minimally intrusive monitoring systems. These qualities make fNIRS suitable for the study of both motor stimuli and cognitive-related hemodynamic changes in the brain [2, 3, 4]. Photon–

tissue interface issues have led the fNIRS researchers to mainly focus their designs onto two types of probes. The main concern in all the probes is the presence of hair on the scalp. Hence the first design includes the LED's and photodetectors and this probe can be directly placed on the forehead but not anywhere else. Furthermore, animal imaging requires miniaturized source and detectors to be placed on animal surface but there are no such components manufactured. Whereas, the use of fiber-coupled sources and detectors have allowed the investigation of cortical hemodynamics that lie underneath places covered with hair and also allowed the examination of the hemodynamic changes on the animal muscles.

The objective of the thesis is to develop a fiber-coupled two-wavelength and four-photodetector spectroscopy system for the detection of cortical hemodynamic changes occurring during motor and visual tasks as well as for the study of animal hemodynamics. The work involves completing its construction, evaluating the instrument performance, and performing preliminary experimental studies.

1.2 Outline of the Thesis

In writing this thesis, it is attempted to provide a thorough background of the medical, physical and technological aspects of available near infrared imaging systems. A large section of the thesis is dedicated to discussion of the system's design features, especially lasers and their drivers. Finally, system verification is performed by the results from the phantom measurements and experimental studies. However, since the expected source-detector distance can not be achieved, human brain activation measurements have not been performed yet.

Chapter 2 provides a general introduction to the physics and mathematics of light propagation through biological tissue and summarizes the history and current state of NIR spectroscopy and imaging systems. The most common types of instruments are reviewed, and compared.

Chapter 3 begins with a discussion of the system design considerations and requirements. A brief explanation of the functioning of the instrument as a whole is followed by a detailed description of the individual optical and electronic assemblies, as well as the data acquisition components and software.

In Chapter 4, system characteristics and its performance are tested and some preliminary experimental studies are performed to check its suitability for the investigation of hemodynamic response during brain activity and muscle activity in human and animal.

Finally, Chapter 5 provides a discussion of the work done so far and the prospects for the future of this project.

2. NEAR INFRARED SPECTROSCOPY (NIRS)

2.1 Principles of Near Infrared Spectroscopy

Jobsis (1977) discovered an optical window in the near-infrared spectrum allowing light, within this range, to usefully penetrate the intact cranium and reach sufficient depths to probe the surface of the cerebral cortex [5]. Such NIR studies can be performed either by trans-illumination methods or in reflectance mode. Trans-illumination is possible if the diameter of the object to be imaged is relatively small allowing light to enter in one side, traverse the sample and exit from the opposite surface e.g. a forearm. However in the case of larger samples, such as an adult head, reflectance mode must be used. Light entering the head at a particular point becomes diffuse as the photons undergo multiple scattering events. A number of photons are absorbed while others continue to be scattered following a random walk path movement through the medium. Some photons may be back-reflected from tissue and exit the surface up to several centimetres from the original point source location, as shown in figure 2.1. These back-reflected photons may be detected and analysis of the detected light signal over time can reveal optical properties of the tissue. Both experimental and theoretical studies have shown that the photons travel in an arcshaped or “banana-shaped” path from source to detector (Figure 2.1) [6]. Changes in tissue oxygenation associated with brain activity modulate the absorption and scattering of these NIR photons and hence affect the detected light levels emerging from the tissue. Thus, through measurement of optical changes at various wavelengths in the NIR band, qualitative measures of brain activity can be obtained.

The NIR response in the brain encompasses two signals. A slow response (approx. 5-8sec) results from attenuation changes due to cerebral hemodynamic changes in blood volume and oxygenation. This signal is an indirect indicator of neuronal activity, related through neurovascular coupling. There is also a fast response, which occurs on the order of milliseconds and is thought to be due to changes in the scattering properties of the neuronal membranes during firing [7, 8]. This signal is more directly related to neural activity and may correlate with evoked potentials commonly used in EEG analysis. It has been termed

the Event Related Optical Signal [9]. Given the two types of responses discernible in the NIR signal, the methodology has the capacity to examine both vascular and neuronal responses, making it a worthy approach for investigating neurovascular coupling phenomena. In order to interpret the optical signal it is helpful to first consider the nature of light propagation.

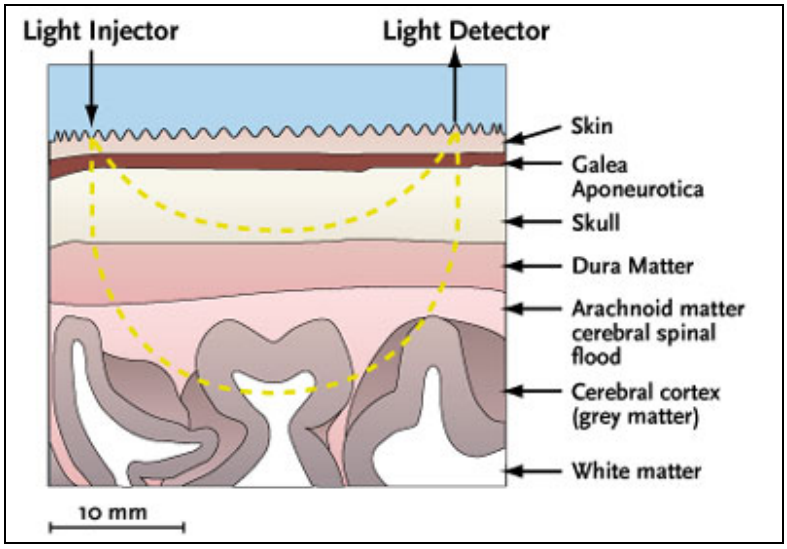

Figure 2.1 An illustration of light pathway in tissue [10].

2.2 The Nature of Light Propagation

Photons propagating through a medium can either pass through unperturbed, be absorbed or be scattered by molecules in the medium. Figure 2.2 outlines the propagation of photons though a scattering and absorbing medium. From this diagram it is clear that scattering and absorption effects attenuate the detected light signal. The attenuation due to absorption effects can be described by a mathematical formulation known as the Beer Lambert Law. Attenuation due to scattering effects is taken into account using a modified version of this law [11].

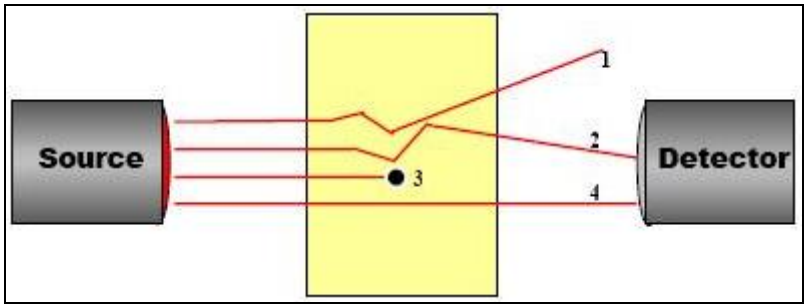

Figure 2.2 Light interaction with a scattering and absorbing medium. Photons 1 and 2 both are undergo scattering events but only photon 2 arrives at the detector; Photon 3 is absorbed; Photon 4 is ballistic nature, i.e. unaffected by scattering or absorption [11].

2.2.1 Absorption, Beer-Lamber Law

The *absorption coefficient*, μ_a (in units mm^{-1}), can be defined by the following equation (Eq. 2.1) where dI is the differential change of intensity I of a collimated light beam traversing an infinitesimal dx through a homogeneous medium with an absorption coefficient μ_a.

$$dI = -\mu_a I dx \tag{2.1}$$

Integration over a thickness x yields

$$I = I_0 e^{-\mu_a x} \tag{2.2}$$

The absorption coefficient can also be expressed in terms of particle density ρ and absorption cross section σ_a giving the *Beer-Lambert* law (Eq. 2.3)

$$I = I_0 e^{-\rho \sigma_a x} \tag{2.3}$$

The reciprocal, $1/\mu_a$, is called the *absorption pathlength* and equals the mean free path a photon travels between consecutive absorption events. Another quantity that is commonly used is the *specific extinction coefficient* ε(λ), which represents the level of absorption per μmol of compound per litre of solution per cm (usually quoted in units

μmolar^{-1} cm^{-1}). It is defined using base 10 logarithm units, and can be related to the absorption coefficient via the Eq. 2.4 where c is the concentration of the compound (in units of μmolar).

$$\varepsilon(\lambda) = \log_{10}(e)\frac{\mu_a}{c} \tag{2.4}$$

The *transmission*, *T*, is defined as the ratio of transmitted to incident intensity

$$T = \frac{I}{I_0} \tag{2.5}$$

and the *attenuation*, or *optical density* (OD) of an attenuating medium is given by the Eq. 2.6 and Eq. 2.7 [12, 13].

$$OD(\lambda) = \log_{10}(1/T) = -\log_{10}(I/I_0) \tag{2.6}$$

$$OD(\lambda) = \log_{10}(e)\mu_a x = \varepsilon(\lambda)cx \tag{2.7}$$

2.2.2 Scattering

Light interaction with biological tissue is greatly affected by scattering events. Scattering is a result of mismatch between regions of different refractive indices. In tissue it occurs due to mismatch between intra-cellular and extra-cellular fluid, membrane boundaries, and also from particles such as mitochondria, ribosomes, fat globules and glycogen. Scattering of NIR photons is primarily due to elastic collisions, i.e. the photon changes direction but there is no energy lost during the collision. In a non-absorbing medium light attenuation due to scattering alone would be expressed by Eq. 2.8

$$I = I_0 e^{-\mu_s x} \tag{2.8}$$

where μ_s is the scattering coefficient.

The skull is a highly scattering tissue even though it has very low absorption properties. The photon's pathlength is increased as a result of scattering events. In the adult head the average photon pathlength is typically six times the distance between the light source and detector. This extended pathlength also leads to scattering losses – the longer a photon remains in the tissue the higher chance it has of being absorbed. In order to accommodate these events the Beer-Lambert Law is modified by integrating a differential pathlength factor and a term to account for scattering losses (Eq. 2.9). The term G is governed by the measurement geometry of the system.

$$OD(\lambda) = \log_{10} \frac{I_0}{I} = \varepsilon(\lambda) cLB + G \qquad (2.9)$$

where is L is the distance between the source and detector, B is the differential pathlength factor and G is a term to account for scattering losses.

2.3 Light Propagation Through Biological Tissue

Absorption and scattering are the two physical phenomena affecting light propagation in biological tissue (Figure 2.3). Although both are important, scattering is the dominant mechanism. Even for thin, sub-millimetre, sections of tissue, injected photons are likely to be scattered several times before they reach the boundary. As a consequence a coherent, collimated input laser beam will be effectively incoherent and isotropic after traversing a few millimetres of tissue. Absorption, and to a lesser extent scattering, are wavelength dependent. Moreover, the concentration of some of the absorbers (chromophores) varies in time, reflecting physiological changes in the tissue. Most importantly, hemoglobin, the oxygen-carrying molecule of the red blood cells, shows a strong oxygenation state dependent absorption profile. The refractive index varies very little on a macroscopic scale and is typically around 1.40 for most tissue types. The

refractive indices of the individual tissue constituents vary from 1.33 for water to approximately 1.55 for fat and concentrated protein solution [12].

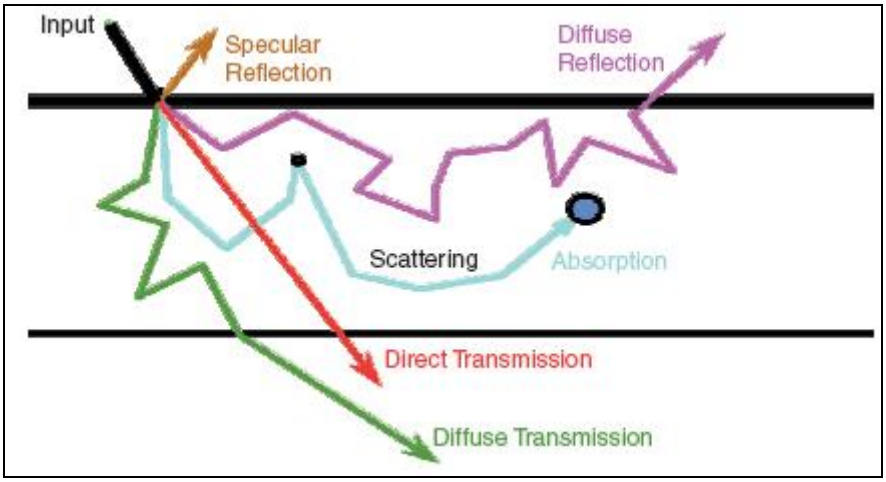

Figure 2.3 Paths of photons through tissue [14].

2.3.1 Chromophores in Biological Tissue

The main constituents of biological tissue which contribute towards absorption in the near infrared are water, fat and hemoglobin. While the former two remain fairly constant over short time-scales, the concentrations of oxygenated and deoxygenated hemoglobin change according to the function and metabolism of the tissue. Thus the corresponding changes in absorption can provide clinically useful physiological information. This section discusses the absorption properties of these tissue constituents as well as measurements of the absorption and scattering coefficients of a variety of specific tissues [15].

2.3.1.1 Water. The absorption spectrum of water in the range 600-1050 nm is shown in Figure 2.4. Significant transmission through tissue is only possible from the UV (about 200 nm, not shown in spectrum) to the near infrared (about 935 nm). The absorption drops again beyond 1000 nm, but there are currently no efficient detectors available at such long wavelengths.

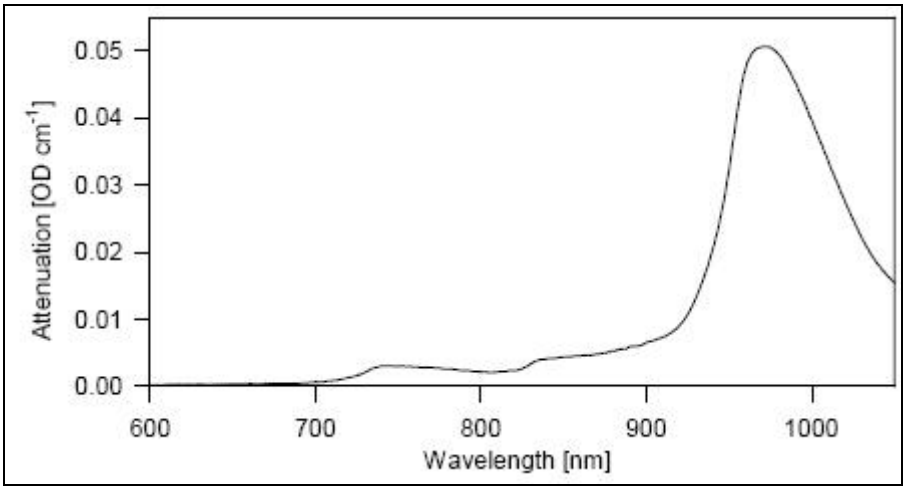

Figure 2.4 Absorption spectrum of water [15].

Note that although the absorption coefficient of water is rather low in this 'water transmission window', it is still a significant contributor to the overall attenuation as its concentration is very high in biological tissue. The average content in the neonatal brain is 90%, and 80% in the adult brain [13, 15].

2.3.1.2 Lipid. Figure 2.5 represents the absorption spectrum of pork fat, which is thought to be largely identical to that of human lipids. The absorption coefficient, which is of the same order of magnitude as for water, is low at shorter wavelengths (down to about 600 nm, not shown in spectrum), with a strong peak at about 930 nm. However, because of the low content of lipids in the brain, the effect on the overall absorption is rather small [13, 15].

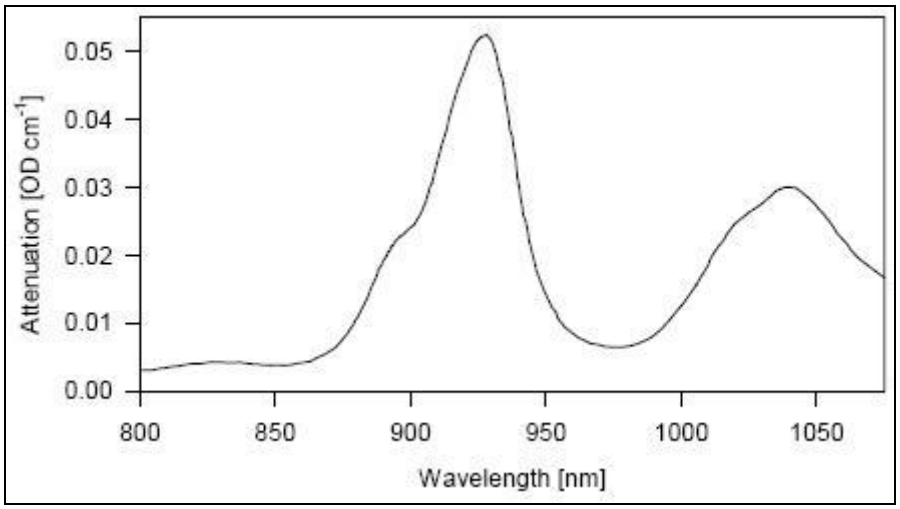

Figure 2.5 Absorption spectrum of fat [15].

2.3.1.3 Hemoglobin. Hemoglobin molecules within the red blood cells (Erythrocytes) carry 97% of the oxygen in the blood, while the remaining 3% is dissolved in the plasma.

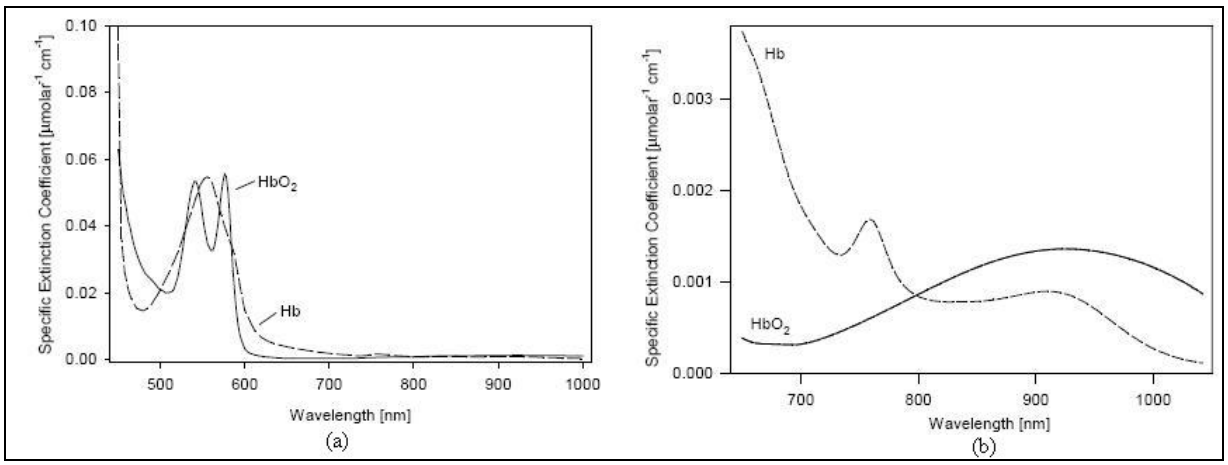

Figure 2.6 Absorption spectra of oxy, deoxyhemoglobin in the ranges 450-1000nm (a),and 650-1050nm (b) [15].

Each hemoglobin molecule consists of four iron-containing haeme groups as well as the protein globin. It is the iron to which the oxygen atoms easily bind, causing the hemoglobin molecule to assume a new three-dimensional shape. In the oxygenated state hemoglobin is referred to as *oxyhemoglobin* (HbO2), and in the reduced state it is called *deoxyhemoglobin* (Hb).

The spectra of oxy- and deoxyhemoglobin, expressed in terms of the specific extinction coefficient, can be seen in Figure 2.6. While both absorb strongly in the blue and green regions of the visible spectrum, the absorption of deoxyhemoglobin is slightly stronger beyond about 690 nm. Hence venous blood appears in a darker red than the arterial blood. Note the isobestic point at about 800 nm, where the two curves intersect. If one is able to accurately determine the tissue absorption coefficients at, say, 20 nm, to either side of this wavelength it is then possible to determine both blood volume and oxygenation. The strong increase in absorption below 600 nm sets a lower limit for spectroscopic or imaging measurements.

There is a number of other tissue chromophores, such as melanin, cytochrome c oxidase, myoglobin, etc. These can be largely ignored in the near infrared (but not in the visible!) regime, as they contribute little to the overall attenuation. The combined ‘absorption window’ lies in the range 600-900 nm. Taking into account the increase in

scattering at lower wavelengths and a rapid drop in quantum efficiency of practical detectors at longer wavelengths, the 'useful' range is approximately 650-900 nm [15].

2.3.2 Theory of Modified Beer-Lambert Law, Hb, HbO_2 Calculations

The modified Beer–Lambert law is typically used to describe the change in light attenuation in scattering media because of absorption changes (which in turn result from changes in chromophore concentrations). When the change in absorption is global throughout the medium, then the MBLL is written as

$$\Delta OD(\lambda) = (\varepsilon_{HbO_2}(\lambda)\Delta[HbO_2] + \varepsilon Hb(\lambda)\Delta[Hb])LB(\lambda) \tag{2.10}$$

where ΔOD(λ) is the change in optical density measured at a given wavelength, *L* is the separation between the source and detector, and B(λ) is the differential pathlength factor (unitless), which accounts for the increased distance that light travels from the source to the detector because of scattering and absorption effects (in the presence of no scattering B(λ)=1). As shown in, the change in absorption is related to changes in the chromophore concentrations of oxy-hemoglobin (Δ[HbO_2]) and deoxy-hemoglobin (Δ[Hb]) by the extinction coefficients $\varepsilon_{HbO2(\lambda)}$ and $\varepsilon_{\Delta Hb(\lambda)}$, which are wavelength dependent. From measurements of ΔOD(λ) at two wavelengths, and assuming $B(\lambda_1)\approx B(\lambda_2)=B$, chromophore concentrations of oxy-hemoglobin (Δ[HbO_2]) and deoxy-hemoglobin (Δ[Hb]) can be calculated as:

$$\Delta[Hb] = \frac{OD(\lambda_1)\varepsilon_{HbO_2}(\lambda_2) - OD(\lambda_2)\varepsilon_{HbO_2}(\lambda_1)}{LB(\varepsilon_{Hb}(\lambda_1)\varepsilon_{HbO_2}(\lambda_2) - \varepsilon_{Hb}(\lambda_2)\varepsilon_{HbO_2}(\lambda_1))} \tag{2.11}$$

$$\Delta[HbO_2] = \frac{OD(\lambda_1)\varepsilon_{Hb}(\lambda_2) - OD(\lambda_2)\varepsilon_{Hb}(\lambda_1)}{LB(\varepsilon_{HbO_2}(\lambda_1)\varepsilon_{Hb}(\lambda_2) - \varepsilon_{HbO_2}(\lambda_2)\varepsilon_{Hb}(\lambda_1))} \tag{2.12}$$

from which total blood volume change and oxygenation can be estimated by Eq. 2.13 and Eq. 2.14, respectively.

$$\Delta[BV] = \Delta[HbO_2] + \Delta[Hb] \tag{2.13}$$

$$\Delta[Oxy] = \Delta[HbO_2] - \Delta[Hb] \tag{2.14}$$

2.4 Near-Infrared Spectroscopy Instrumentation Principles

While the underlying principle of NIR techniques remains the same throughout, each NIR research group has taken its own approach in developing NIR imaging systems in accordance to its desired applications. There are three approaches to NIRS instrumentation - Continuous Wave, Time-Resolved Spectroscopy and Frequency Domain or Phase-resolved Techniques. These techniques are explained briefly and compared with their own advantages and disadvantages. Then, a variety of instruments currently in use for both commercial and research applications are introduced.

2.4.1 Continuous Wave

The simplest method of NIRS to implement is continuous wave. In this mode the light source is switched on constantly and magnitude changes in the detected light signal are used to evaluate tissue attenuation. Systems using light sources modulated at low frequencies (a few kilohertz) are also considered to be continuous wave. The light source is typically a laser or LED but halogen lamps have also been used. The attenuation of light is the only parameter measured by this method. Light detectors used for this purpose include sensitive photodiodes, avalanche photodiodes (APDs), photomultiplier tubes (PMTs) or charge coupled devices (CCD). The continuous wave approach can be implemented easily on account of its simplicity and flexibility, however it cannot make accurate quantitative measurements of chromophore concentrations. This is because a direct measurement of photon pathlengths cannot be made, and therefore the differential pathlength factor must be estimated based on previous studies [16]. Quantitative measurements rely on the

differential pathlength factor being measured using either time resolved spectroscopy or frequency domain methods.

2.4.2 Time Resolved Spectroscopy

Time resolved spectroscopy measures the time taken for photons to traverse a medium termed time of flight. This type of formulation has been used in the past to determine the thickness of clouds. Laser pulses broaden after propagation though thick clouds due to multiple scattering events. The temporal response of a detector to a delta function shaped laser pulse propagating through a cloud can be used to determine the thickness of the cloud [12, 16]. This theory can be applied to measurements in tissue using a simple time of flight approximation to calculate the differential pathlength, i.e. total distance traveled through the tissue, given by Eq. 2.15.

$$B = vt \tag{2.15}$$

where B is the differential pathlength, t is the time taken for an optical pulse to be transmitted through a medium, and v is the speed of light within the medium [16].

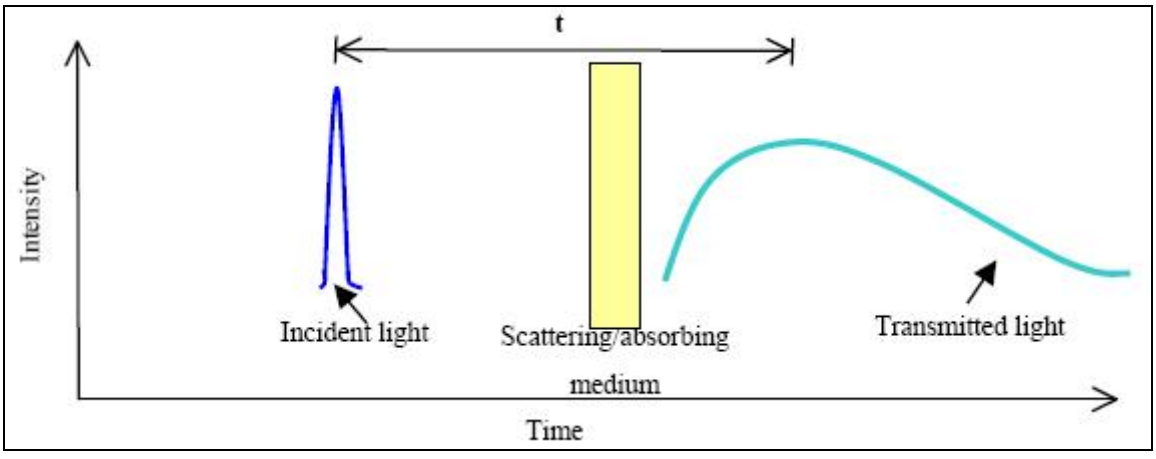

Figure 2.7 Time-resolved spectroscopy. A short pulse of incident light is broadened and attenuated by the medium [11].

In order to measure the time of flight, *t,* time-domain systems employ a light source capable of emitting short picosecond pulses of light and a photodetector that can capture

the distribution of photon arrival times, e.g. a streak camera. The temporal distribution of the detected signal provides information about the optical interaction with tissue, i.e. scattering and absorption effects [17]. Figure 2.7 shows the temporal spread of the transmitted light signal.

2.4.3 Frequency Domain Measurements

By Fourier theory, the same information attained using a time-domain approach can also be calculated by using a frequency domain approach. In this case the light source is modulated at very high frequency (hundreds of megahertz). Light migrating through tissue undergoes both amplitude and phase shifts as shown in figure 2.8. The transmitted optical signal is detected at the same modulation frequency but with a phase shift that can be measured using phase sensitive detection techniques [18]. The phase delay is related to the average time of flight of the photons. The differential pathlength in this case is given by Eq. 2.16.

$$\beta = \frac{\phi \cdot c}{2\pi \cdot f} \tag{2.16}$$

where ϕ is the phase shift, c is the speed of light within the medium and f is the modulation frequency of the light source [11].

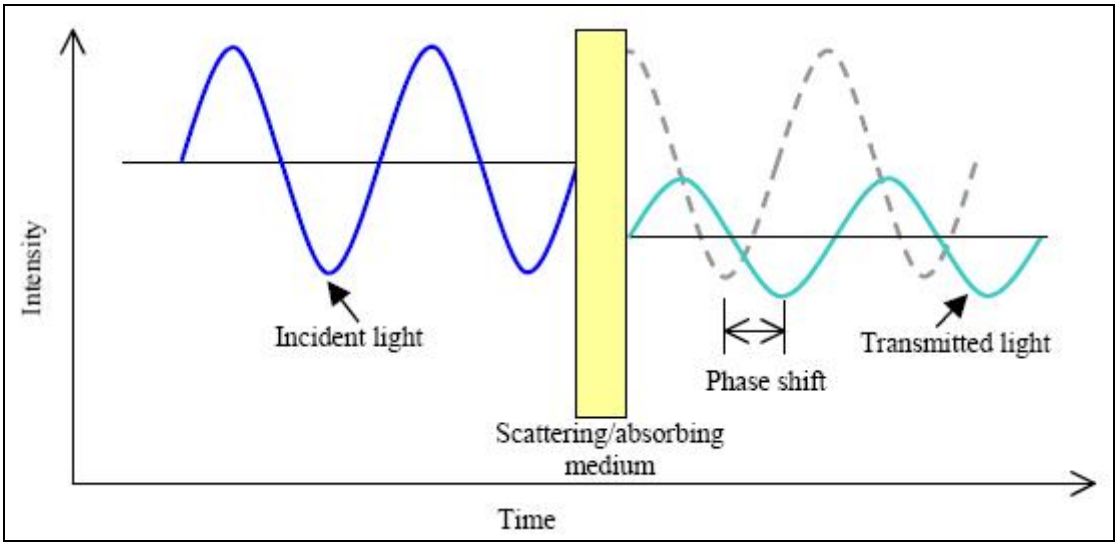

Figure 2.8 Frequency domain measurements. Incident light modulated at high frequency (MHz) undergoes phase shift and amplitude decay [11].

2.4.4 Comparison of the Methods

The choice of the measurement method is determined by the type of information sought and availability of system. Each of the measurement methods, CW, FD and TR, has its own advantages and disadvantages outlined in Table 2.1.

Table 2.1 Comparison of the NIRS system methods.

METHODS	ADVANTAGES	DISADVANTAGES	INFORMATION COLLECTED
Continuous Wave	Sampling rate, Instrument size, Cost	Penetration depth, Difficult to separate, Absorption and scattering	Finger pulse oximeter, Neuroimaging studies,
Time-Resolved	Spatial resolution, Penetration depth, Most accurate separation of absorption and scattering	Sampling rate, Instrument size, Stabilization, Cost	Imaging cerebral oxygenetation, and hemorrage in neonates, breast imaging
Frequency Domain	Sampling rate, Relatively accurate separation of absorption and scattering	Penetration depth	Cerebral and muscle oximetry, Breast imaging, Tissue characterization

2.4.5 NIRS Instruments Currently In Use

Today, there is a wide variety of instruments currently in use for both commercial and research applications;

Hitachi (Japan) have built a continuous intensity system for the topographic mapping of cortical activity (ETG-4000). The measurements were performed with a continuous wave optical imager system, which was placed on the head to obtain a topographic map and it collects simultaneous data through 48 channels. TechEn Inc. (the USA) developed a continuous wave near-infrared spectroscopy system. The system is based on proprietary digital-imaging technologies developed at TechEn, Inc. and clinical research conducted at Massachusetts General Hospital.. The Continuous Wave 32 is a 32-channel system with 32 source-detector pairs and 2 to 16 different laser wavelengths. This system is used both to collect data and to produce images of hemodynamic activity. Imaging is made possible by the increased number of channels. ISS Inc. (the USA) developed a frequency domain NIRS system (OxiplexTs). Light of two different wavelengths is used and the light is modulated at an RF frequency of 110 MHz. The collected light is measured and processed, and the absorption and scattering coefficients of the medium are determined. There are 8 laser diodes emitting at 690 nm and 8 laser diodes emitting at 830 nm. Laser diodes are time multiplexed. Somanetics Inc. (the USA) developed the INVOS cerebral oximeter which passes harmless, low-intensity near-infrared light into the patient's forehead where it penetrates the skull and passes through the cerebral cortex. By measuring the returned light at two distances from the light source (3 and 4 cm), the spectral absorption of blood in the brain can be determined. The INVOS Cerebral Oximeter generates two wavelengths of light (730 and 805 nm) using two LEDs (light-emitting diodes) which are alternately illuminated. Hamamatsu Inc. (Japan) developed a continuous wave nirs system. There are 3 laser diodes at different wavelengths as the light source. They are coupled to fiber optic cables and light is also collected by fiber cables.

The group of Dr. B. Chance at the University of Pennsylvania, have constructed a continuous wave light optical imager that consists of ten detectors and four light sources arranged in an array. This device is placed on the forehead to measure the optical density

changes during the brain activition. Another system developed in Prof. Chance's group is an 8 channel time resolved TCSPC instrument is also developed. The system employs pulsed laser diodes at 780 and 830 nm to perform spatially resolved NIR spectroscopy for monitoring motor cortex activity, as well as performing tomographic breast phantom studies. At Dartmouth College Dr. H. Jiang has developed both continuous intensity and frequency-domain optical imager. At University College London, the research group, under the direction of Professor David Delpy, is involved with the development of new optical monitoring instruments based on Time-resolved optical imaging system for medical applications. At Harvard Medical School, Dr. D. Boas's group has constructed a continuous wave optical imager. Dr. Anreas Hielscher's biomedical optics group at Columbia University is developing numerical and experimental techniques for in vivo tissue diagnostics. A frequency domain NIRS system at Dublin City University was developed. They use leds for lighting sources and 3mm fibers for light collection. Also, they designed a new optode for proper placement on the head. Dr. D. Benaron's research group at Stanford University developed an optical imaging system that uses pulsed laser diode sources and either a commercially available Optical Time Domain Reectometer (OTDR) or avalanche photodiode detectors (APD).

Here at Bogazici University, Dr. Ata Akin, and Uzay Emir developed a NIRS system (NIROXCOPE) to examine the cognitive changes in the prefrontal cortex [13]. In order to study the remaining parts of the brain which is hairy, a fiber optic based system (described in the next chapter) is needed.

3. SYSTEM DESIGN

The fundamental components of any NIR system are the light source and detector. To complete the system driving electronics, amplification and data acquisition methods are carefully chosen according to the demands of the relevant application. As discussed in Chapter 2 there are three ways of performing NIR measurements – Continuous Wave, Time Resolved Spectroscopy and Frequency domain methods. In this thesis, we implemented a continuous wave nirs system because of its flexibility and low cost (Figure 3.1). We used two laser diodes with different wavelengths (785 – 850nm), modulated at different frequencies to be able to separate them properly at the receiver side. To be able to couple the lasers to the fiber optic cables, optical converters were used. At the receiver side, light scattered from the tissue are received by fiber optics and sent to near infrared wavelength sensitive photodiodes. Then, current is converted to voltage and amplified by the transimpedance amplifiers whose output is filtered by notch filters to eliminate the 50 Hz signal from the mains. At the end, the analog signal is converted to digital signal by daqcard to analyze the modulated output signals on the computer. In the following sections, detailed descriptions of the subunits will be given.

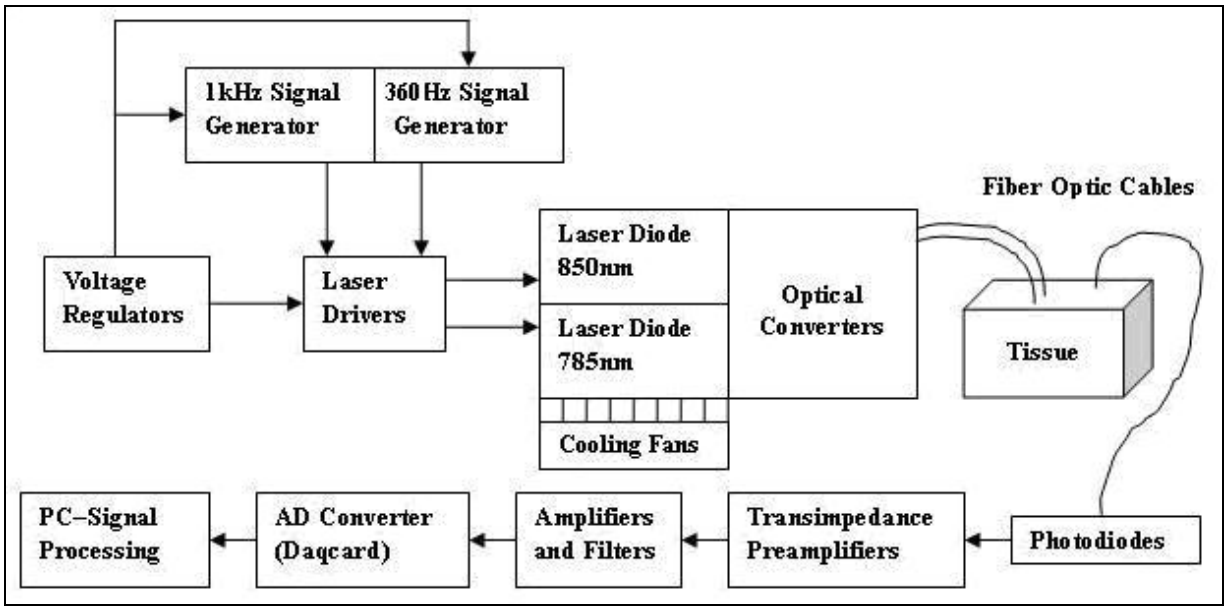

Figure 3.1 Block diagram of the NIRS system.

3.1 Power Supply

Switch mode power supply (SMPS) unit is manufactured by Philips Corporation and it provides 12 V_{DC} output voltage and 2.8 A output current at maximum load. It has input voltage range 100-240 V_{AC} and it has overvoltage and overload protection. The unit is used to provide the operating currents for the diode lasers, drivers, amplifiers and cooling fans.

3.2 Voltage Regulators

Laser diodes operating voltage is approximately 2.5 V_{DC}, therefore it is need to regulate the laser diode driver supply voltages. To perform this, LM317 positive adjustable regulator is used (Figure 3.2). It can supply more than 1.5 A of the load current with an output voltage adjustable over a 1.2 to 37 V.

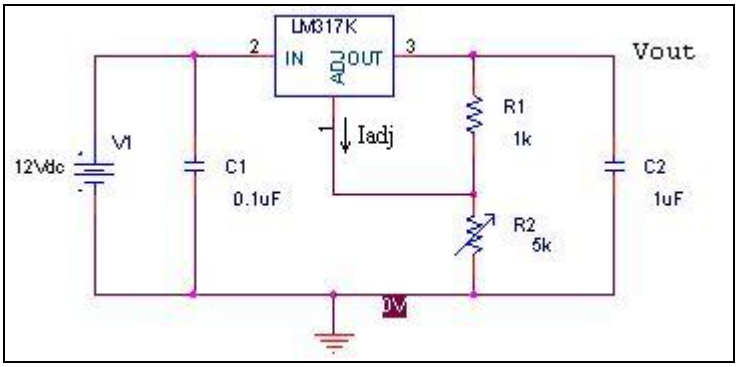

Figure 3.2 Schematic of a voltage regulator circuit.

The input output relationship is given in Eq. 3.1.

$$V_{OUT} = 1.25\left(1 + \frac{R_2}{R_1}\right) + I_{ADJ} R_2 \tag{3.1}$$

As the drivers need approximately 2.5 Volts, R_2 and R_1 are chosen as 5k adjustable and 1k, respectively. This enables to be able to adjust the output voltage as desired in the range 1.25 – 7.5 Volts. Since I_{ADJ} is controlled to less than 100µA, the error associated with this term is negligible in most applications.

3.3 Voltage Converter

Since sine wave generators and their amplifier need minus supply voltage a monolithic CMOS switched-capacitor voltage converter (LTC1144) is used. It performs supply voltage conversion from positive to negative from an input range of 2V to 18V, resulting in complementary output voltages of –2V to –18V. In the circuitry, its function is to convert 12 V_{DC} to -12 V_{DC} (Figure 3.3).

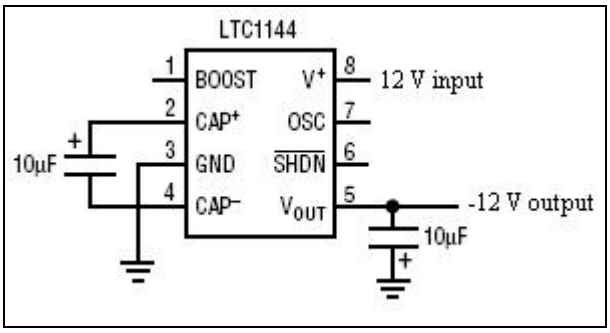

Figure 3.3 Generating -12 V from 12V.

3.4 Sine Wave Generators

In order to modulate the laser currents, the ICL8038 monolithic integrated circuit capable of producing high accuracy sine waves is used. The frequency can be selected externally from 0.001Hz to more than 300kHz using either resistors or capacitors. The output voltage of ICL8038 is typically $0.22xV_{SUPPLY,}$ so V_{p-p} will be 5.28V (0.22x12=2.64 V and 0.22x(-12)=-2.64 V). This voltage swing can be amplified or attenuated by an inverting amplifier by adjusting the 20 K resistor seen in Figure 3.4.

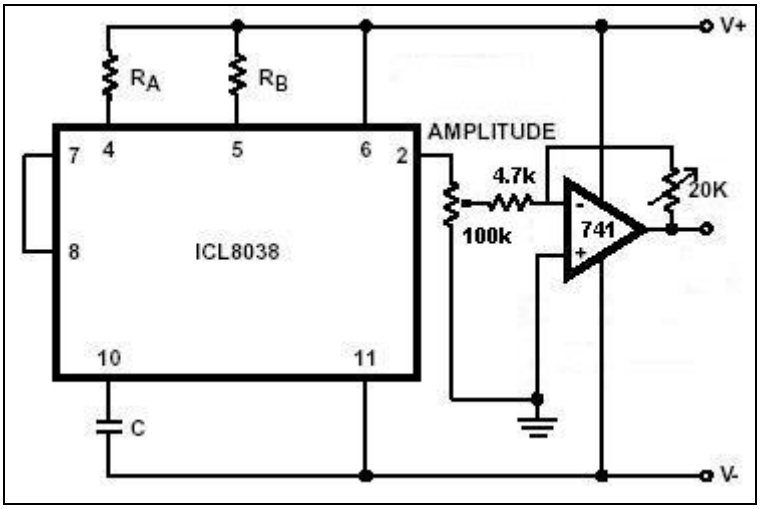

Figure 3.4 Sine wave output buffer amplifier.

The frequency of the sinewave is adjusted by R_A, R_B and C. If R_A=R_B the frequency becomes;

$$f = \frac{0.33}{R \cdot C} \tag{3.2}$$

One of the frequencies for the laser modulation is selected as 1 kHz, so R and C is taken as 100 K and 3.3 nF, respectively. The other modulation frequency is taken as 360 Hz to avoid harmonic crosstalk. Therefore, R is taken as 277 K and C is taken again as 3.3 nF.

3.5 Laser Diodes

Laser Diodes are complex semiconductors that convert an electrical current into light. The conversion process is fairly efficient in that it generates little heat compared to incandescent lights. Five inherent properties make lasers attractive for use in fiber optics.

1. They are small.
2. They possess high radiance (i.e., They emit lots of light in a small area).
3. The emitting area is small, comparable to the dimensions of optical fibers.
4. They have a very long life, offering high reliability.

5. They can be modulated (turned off and on) at high speeds.

Linearity is another important characteristic of laser diodes. It represents the degree to which the optical output is directly proportional to the electrical current input.

Lasers are temperature sensitive; the lasing threshold will change with the temperature. Figure 3.5 shows the typical behavior of a laser diode. As operating temperature changes, several effects can occur. First, the threshold current changes and the threshold current is always lower at lower temperatures and vice versa. The second change that can be important is the slope efficiency. The slope efficiency is the number of milliwatts or microwatts of light output per milliampere of increased drive current above threshold. Most lasers show a drop in slope efficiency as temperature increases. Thus, lasers require a method of stabilizing the threshold to achieve maximum performance. Often, a photodiode is used to monitor the light output on the rear facet of the laser. The current from the photodiode changes with variations in light output and provides feedback to adjust the laser drive current.

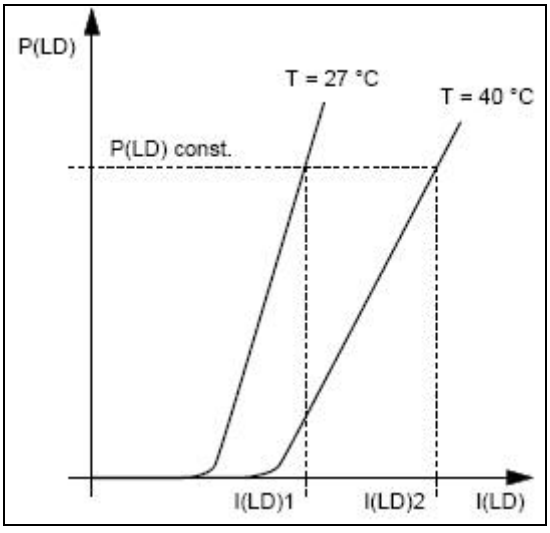

Figure 3.5 Temperature effects on the laser optical output power.

There are two types of laser diodes available today. Automatic power control uses a monitor photodiode feedback that monitors the optical output and provides a control signal for the laser diode which maintains the operation at a constant optical output level. However, in this configuration, there is a risk of overcurrent with self heating and ageing effects of the laser diode. Therefore, cooling is important when using these laser diodes. Lasers with integrated monitor diodes are available in three configurations, all with the

common terminal connected to their housing, which is often electrically connected to the ground (Figure 3.6). In automatic current control, drive circuit that operates the laser diode without a photodiode feedback loop, the laser diode is simply driven at constant current. The optical output will fluctuate as the laser diode temperature changes. So, the temperature must be regulated to maintain a constant output so that it does not exceed critical values.

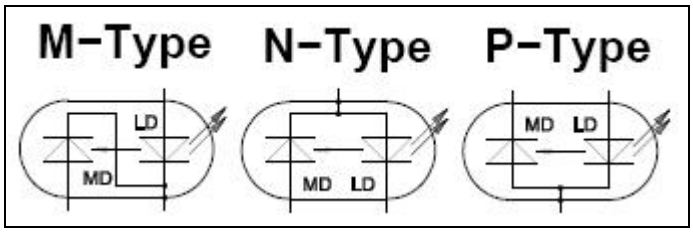

Figure 3.6 Three available diode laser configurations, M-, N-, P-type, require different driver principles.

In this thesis, two laser diodes with monitor photodiodes (N-type) were used. 785nm laser (HL7851G) is manufactured by Hitachi Inc., and 850nm laser (L850P100) is manufactured by Thorlabs Incorporation. HL7851G has a 9.5^0 beam divergence whereas L850P100 has 10^0. The output powers of the lasers were adjusted to give 50 mW by the driver circuits to have the same effect in the tissue [19].

3.6 Laser Driver

As laser diodes in this study have monitor photodiodes to give constant output powers, the drivers should have beenn designed accordingly. Two significant aspects of drivers are to provide the required laser diode current and to be able to process the corresponding monitor current. Additionally, the power supply must match the configuration. Figure 3.7 shows a typical circuitry to drive N type of lasers properly. Current from the integrated monitor diode closes the control loop so that the laser diode generates constant power. The working principle is simple. There are three currents on node M whose voltage value is equal to V_{REF}. They flow over the monitor photodiode(MD), negative input of the opamp and potentiometer R_M. As it is seen, the current over the R_M is equal to V_{REF}/R_M. In the beginning, since the laser diode LD is off, there is no or little current over the monitor photodiode, so all current is flowed out of the

negative input of the opamp to perform Kirchhoff current law at node M. This negative current induces the output of the opamp(input of the tansistor) to increase. As it increases the transistor turns on and the current over laser diode starts to flow and laser diode gives an output power, which causes the current over the monitor photodiode to increase. Therefore, in the next step much lower current is flowed out of negative input of the opamp. This continues until the current out of MD matches the current being sinked by potentiometer, R_M, it also means that it continues until there is no current sinked out of the negative input of the opamp. R_M, usually referred to as the "power adjust" in laser drive circuits, sets the monitor photodiode current.

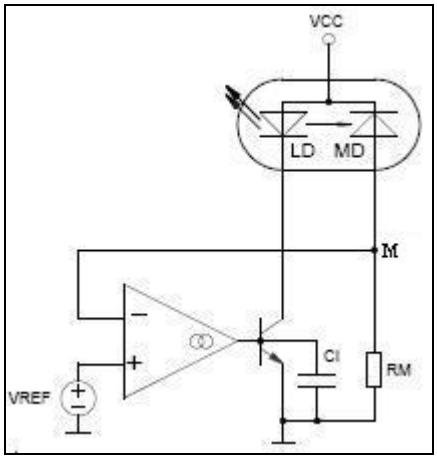

Figure 3.7 Typical N-type laser driver.

Integrated driver circuits offer variety of functions and safety measures and they require few additional components. Therefore, it was better to use an integrated circuit based on the above operational principle. Surely, the drivers (IC-WKN) were selected by matching the features of the laser diodes by IC- HAUS Integrated Circuits Company. It provides laser diode current up to 300mA which is enough for the lasers in this study. It also has the property of permanent shutdown with excessive temperature and overcurrent. Furthermore, it has a modulation input to alternate the output power signal as desired. The internal circuit diagram of the driver is seen in Figure 3.8.

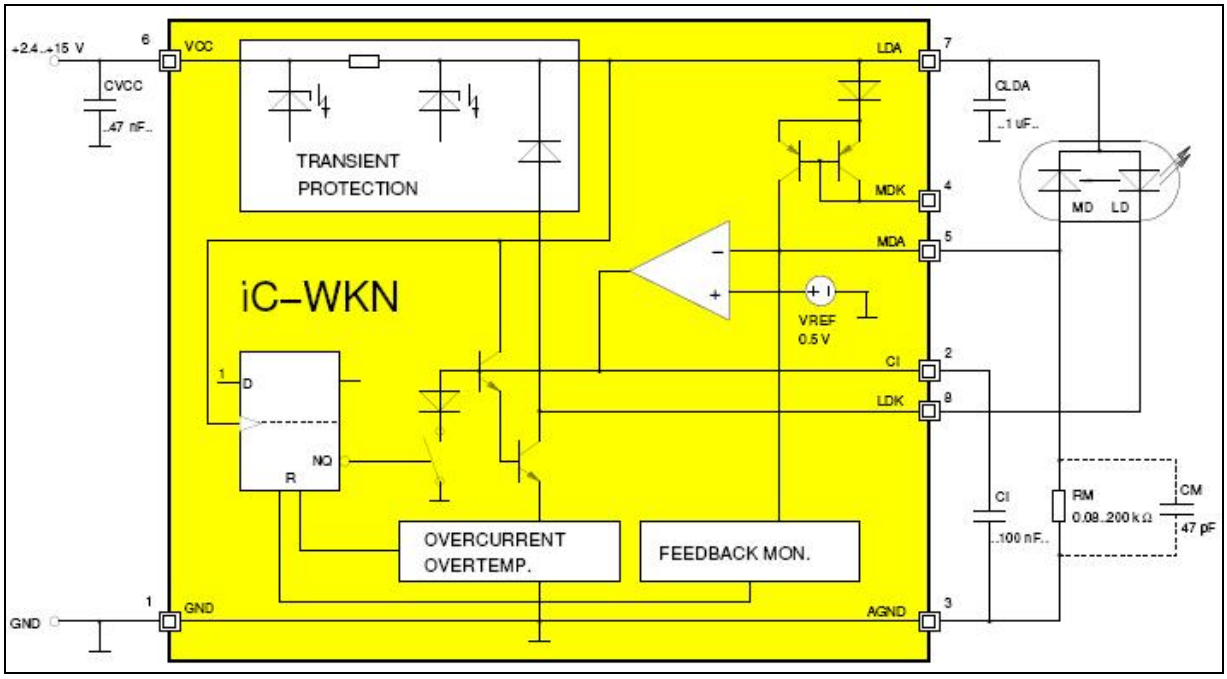

Figure 3.8 Block diagram of the IC-WKN laser driver.

As it is stated above, the power adjustment is performed with the adjustable resistor R_M. Its value is determined by the desired power and current limits of monitor photodiodes MD. In Eq. 3.3 and Eq. 3.4, the calculations of the minimum and maximum values of R_M are shown [20].

$$R_{M\min} = \frac{V_{MDA}}{I_{M\,nom\max}} \frac{P_{nom}}{P_{set}} \tag{3.3}$$

$$R_{M\max} = \frac{V_{MDA}}{I_{M\,nom\min}} \frac{P_{nom}}{P_{set}} \tag{3.4}$$

where $I_{Mnommax}$ and $I_{Mnommin}$ represent the monitor current range at nominal output power P_{nom}, as given in the laser diode datasheet, and P_{set} is the power to be set.

Using the Eq. 3.3 and Eq. 3.4, for the 785 nm diode laser;

$$R_{M\min} = \frac{0.5}{150\mu A} \frac{50mW}{50mW} = 3.3k\Omega\,, \qquad R_{M\max} = \frac{0.5}{25\mu A} \frac{50mW}{50mW} = 20k\Omega\,. \tag{3.5}$$

It is prudent here to divide resistor into a fixed resistor (R_{Mfixed}) and trimmer (R_{Mvar}) for the setup process. Therefore, R_{Mfixed} is chosen as 3.3 kΩ, and R_{Mvar} is taken as 20 kΩ. The same calculation is done for the 850 nm laser and R_{Mmin} is found 666Ω, and R_{Mmax} is 10 kΩ. Therefore, R_{Mfixed} is selected as 670 Ω, and R_{Mvar} is taken as 10 kΩ.

The modulation is performed via the MDK input which modulates the current on the negative input of the opamp. This results in change at the output current of the opamp which is also the current of the laser diode. The maximum allowable modulation current for a hundred percent modulation depth is as that of monitor photodiode. Modulation current is taken as equal to the monitor current in this study for both lasers. Then, in normal operation, the voltages at pin MDK are measured by the voltmeter to determine the V_{mod} and R_{mod}. In Figure 3.7 it is seen that modulation voltage can never exceed the V_{MDK} because of the current mirror inside. Therefore in Eq. 3.6, the second term is always negative or zero making the output power swing at maximum and minimum values [21].

$$P_{OUT} = P_{nom} + P_{nom} \frac{(V_{MOD} - V_{MDK}) / R_{MOD}}{V_{MDA} / R_M} \tag{3.6}$$

For 785 nm laser, because of its low monitor current, R_{mod} is selected as 100 K and peak to peak value of the V_{mod} is adjusted empirically starting from zero to higher values until the sine wave was seen by the detector at 1.5 cm distance on the phantom. For 850 nm laser, the same procedure is done and R_{mod} is selected as 10 K because the monitor photodiode current is not as small as that of 785 nm laser. Again, the amplitude of the sine wave generator is increased until the sine wave at 1.5 cm from the detector is seen. The phantom has the same absorption and scattering characteristics with cerebral cortex.

3.7 Optical Converters

Optical converters were used to make a connection among the electronic circuitry, the lasers and optical fibers. All parts ate manufactured by Thorlabs Incorparation. In Figure 3.9 focusing lens and tubes to focus the laser light inside the fiber optic cable are shown.

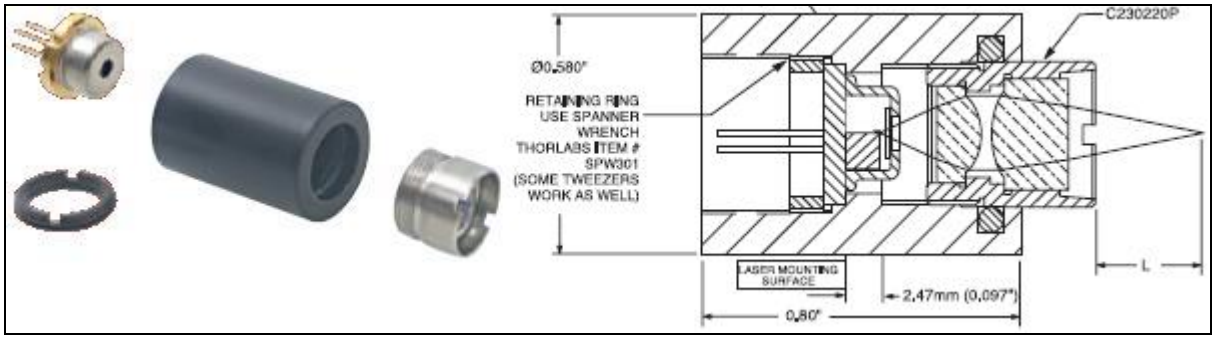

Figure 3.9 Focusing tubes and optics. In the left, laser diode is put into the tube and locked inside. In the right, it is seen that laser light is focused with the lens.

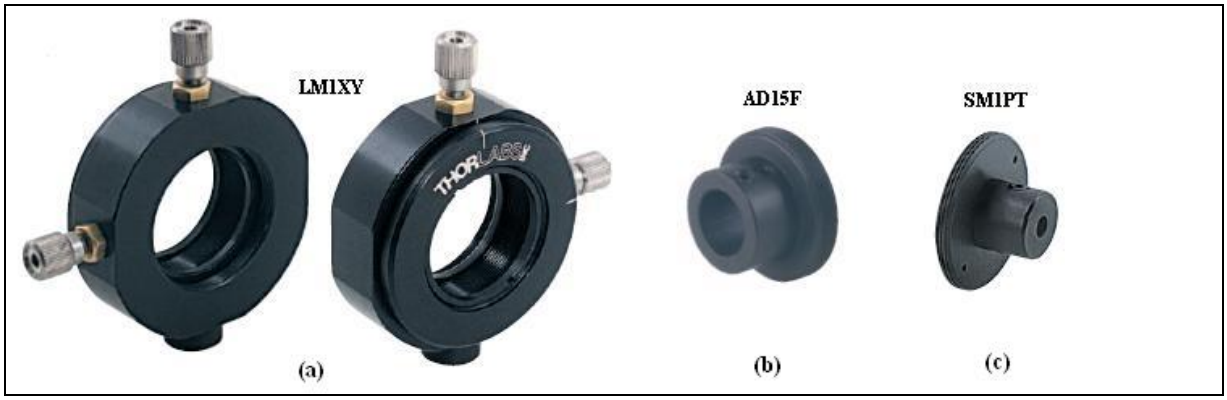

Figure 3.10 (a) Lens mount, (b) Mounting adaptor for focusing tube, (c) Mounting adaptor for optical fibers.

Lens mounts (LM1XY, Figure 3.10a) were used to hold the focusing parts and optical fibers. The focusing tube was inserted in the lens mounts by the ADF15 mounting adaptor (Figure 3.10b), and the optical fibers were mounted on the other side of the lens mounts by SM1PT fiber optic cable adaptor (Figure 3.10c).

3.8 Cooling System

Thermal management of the laser diode is crucial to protect it from excessive heating. The wavelength of the laser light is temperature dependent therefore the temperature of the laser diode must be kept stable to get laser light with constant wavelength. Additionally, as seen in Figure 3.4, the lasing threshold and slope efficiency change with the temperature. Furthermore, the laser diode drivers which have an overcurrent and overtemperature shutdown turn off the laser immediately without the

cooling system. Especially, the lasers in this study runs continuously, cooling system is imperative.

The optical converter part which acts as a heat sink and a powerful air fan which runs continuously solve the problem. With this solution, the laser diodes can give constant output powers for a long time. The temperature tests were done by running them continuously for four minutes and no voltage drop or shutdown occurred. The reason why they are tested in four minutes is the daqcard and PC limitations. These tests were given in the results section.

3.9 Optical Fibers

Since the sensor that gets light in this study is fiber optic cable, fibers with large core diameter are needed. Plastic optical fibers with 3 mm core diameter from Mitsubishi Rayon Company were used because of their availability in the market. The numerical aperture (the light gathering ability) of the fibers is 0.5. Its transmission loss for 650 nm light source is 200 dB/km.

3.10 Photodiodes

The SM05PD1A photodiode by Thorlabs Inc. was used as the photodetector in the circuitry (Figure 3.11). It is a high-speed mounted silicon photodiode with a spectral response from 350 nm to 1100 nm. This photodiode has a PIN structure that provides fast Rise / Fall Times (20 ns) with a bias of 12 V.

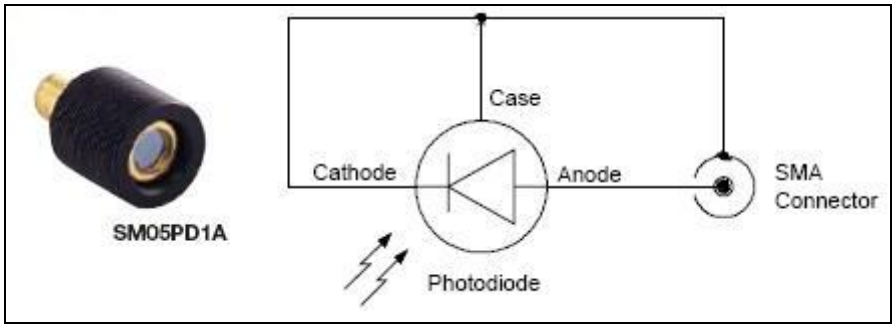

Figure 3.11 The picture and electrical connection of the SM05PD1A.

The Thorlabs SM05PD1A Mounted Silicon-Photodiode is ideal for measuring both pulsed and CW light sources, by absorption of photons or charged particles and generates a flow of current in an external circuit, proportional to the incident power.

3.11 Transimpedance Preamplifiers

Since the photodiode is a kind of current source it is necessary to convert it to voltage. Transimpedance amplifiers (Figure 3.12) are used to perform this. The amplifier has not only this function, but also the function of low pass filtering to eliminate high frequency noise.

The gain of the amplifier is as follows;

$$\frac{V_{OUT}}{I_{IN}} = R_F\left(\frac{1}{1+sR_FC_F}\right) \tag{3.7}$$

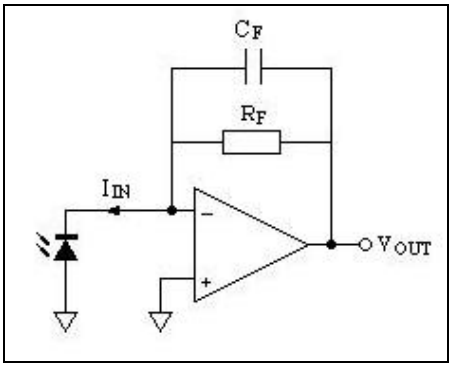

Figure 3.12 – Transimpedance preamplifier.

From Eq. 3.7, the cut-off frequency also called the bandwidth becomes;

$$f_C = \frac{1}{2\pi R_F C_F} \tag{3.8}$$

Although any ac signal above 1 kHz is undesired in the system, using low valued f_C will increase rise time defined as the time required for a pulse to increase from 10% of its final value to 90% of its final value and expressed as;

$$t_R = \frac{0.35}{f_C} \tag{3.9}$$

By considering this fact, the values of R_F and C_F are chosen such that while the circuit eliminates the high frequency noise, it also has a low rise time. The values of R_F and C_F are 1 MΩ and 12 pF respectively. Hence, f_C is approximately 13 kHz and t_R is about 27 μs. From Eq. 3.7, the amplifier gain becomes 1 M with the R_F value. LMC6064, especially designed for photodiode applications, was used as the operational amplifier.

3.12 Notch Filter

The common mode noise (50 Hz) coming from the power line also has to be eliminated. The low pass filter designed as the transimpedance amplifier has no effect on this undesired signal because of the modulation limitations. Therefore, notch filter (Figure 3.13) is also used to suppress 50 Hz signal.

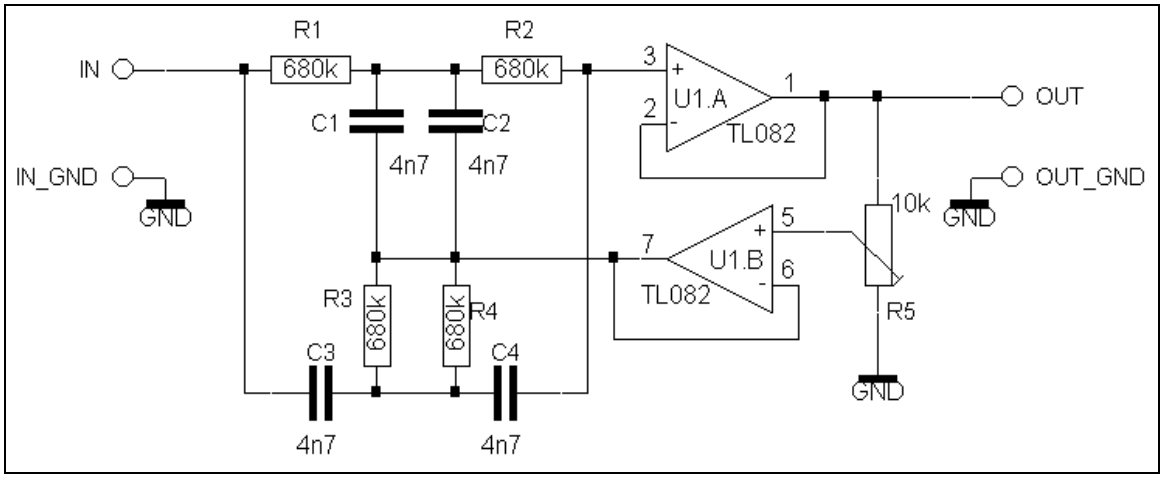

Figure 3.13 Twin T notch filter.

The gain of the amplifier is calculated as;

$$\frac{V_{OUT}}{V_{IN}} = \left(\frac{16(j\pi fRC)^2 + 1}{16(j\pi fRC)^2 + 16(1-X)j\pi fRC + 1} \right) \tag{3.10}$$

where $R=R_3//R_4$ (so $R_1=R_2=2R$), $C=C_1=C_2=C_3=C_4$ and XU1.B is the output voltage of the opamp U1.B which changes with R_5. V_{OUT}/V_{IN} will be zero if the nominator becomes 0. So, $16(j\pi fRC)^2=-1$, then the notch frequency becomes;

$$f = \frac{1}{4\pi RC} \tag{3.11}$$

Hence, R=340 kΩ and C=4.7 nF gives 50 Hz notch frequency.

The simulation result of the output voltage (V_{OUT}) of T Twin notch filter for V_{IN} =1 V as a function of frequency is shown in Figure 3.14.

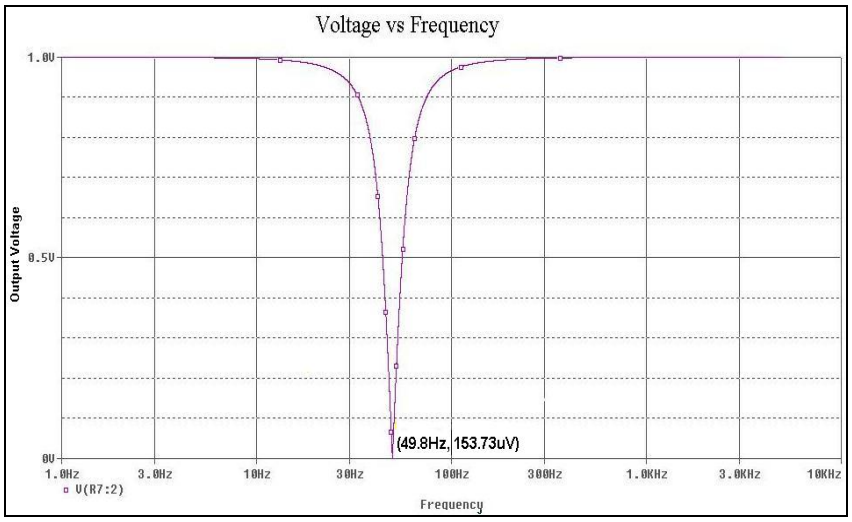

Figure 3.14 The Simulation of the output voltage of the notch filter as a function of frequency.

3.13 Packaging the System into a Portable Case

Components of the system mentioned above were installed to a case to make it portable and robust for easy handling and long time usage. First of all, the PCB of the circuitry was drawn by Orcad Layout program and all the components were soldered carefully. To cool the lasers sufficiently, the lasers were separated from the circuitry inside the case (Figure 3.15). All the optical fiber connections done and necessary buttons were placed on the case. In Figure 3.16 and 17 the front and back views of the case are seen.

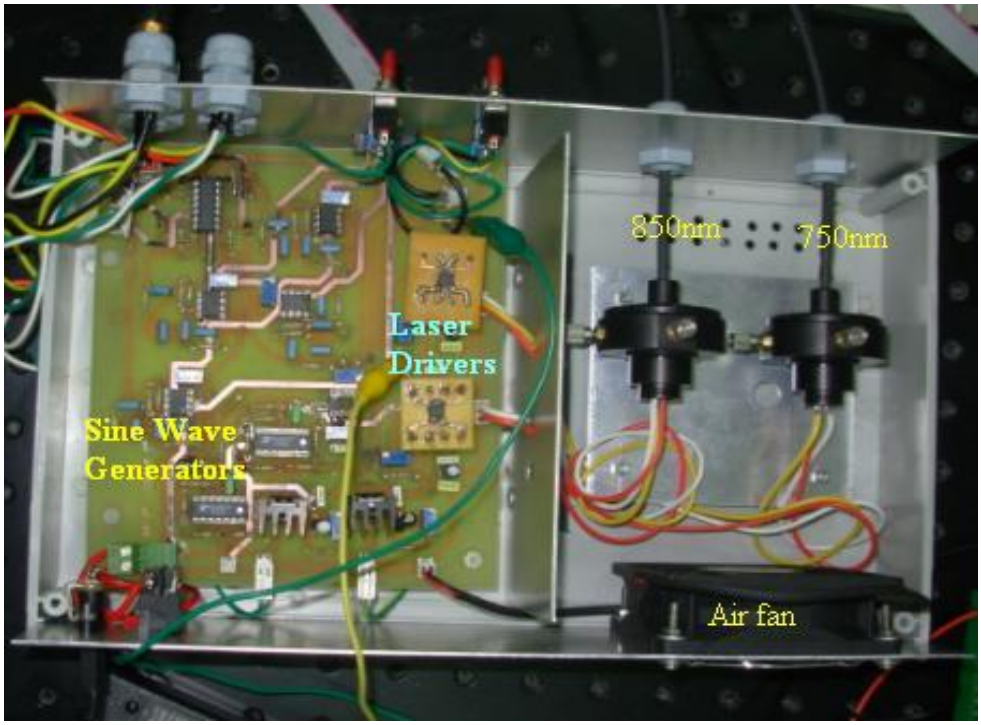

Figure 3.15 Internal view of the case.

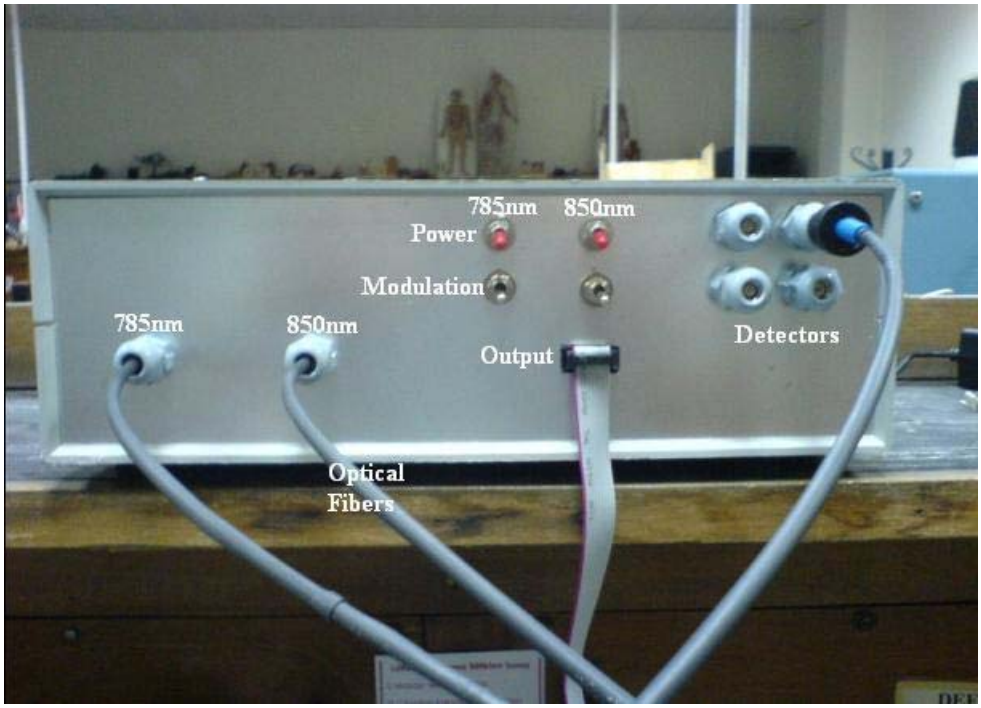

Figure 3.16 The front view of the case.

Figure 3.17 Back view of the case.

3.14 Analog to Digital Converter (DaqCard)

As an data acquisition card, NI PCI-MIO-16E-1 was used. It has a very high sample rate (125000Hz), 16 single or 8 differential analog input channels with 12 bit resolution. As mentioned before, the biggest frequency in the circuitry is 1 kHz, so 10 kHz sample rate is big enough to be able to get the data accurately [22].

The signals were analyzed by the Matlab data acquisition toolbox. The matlab code to initialize the daqcard and to get the data to be analyzed is given in Appendix B. Since there are two signals (360 Hz and 1 kHz) coming to one input, bandpass filters were used in the code to distinguish them and to understand which signal belongs to which laser.

In the next chapter, some system characteristics will be analyzed and some experiments performed will be mentioned to verify the system.

4. SYSTEM VERIFICATION

To verify the system is working properly, photodiode characteristic, temperature dependency, output change with the increasing distance were analyzed and also experimental verification with ischemia in human and rat is performed .

4.1 System Characteristics

4.1.1 Photodiode Output Without Amplifiers

Figure 4.1 shows the raw output of the photodiode in a dark medium. It is apparent that 50 Hz signal from the power line is big.

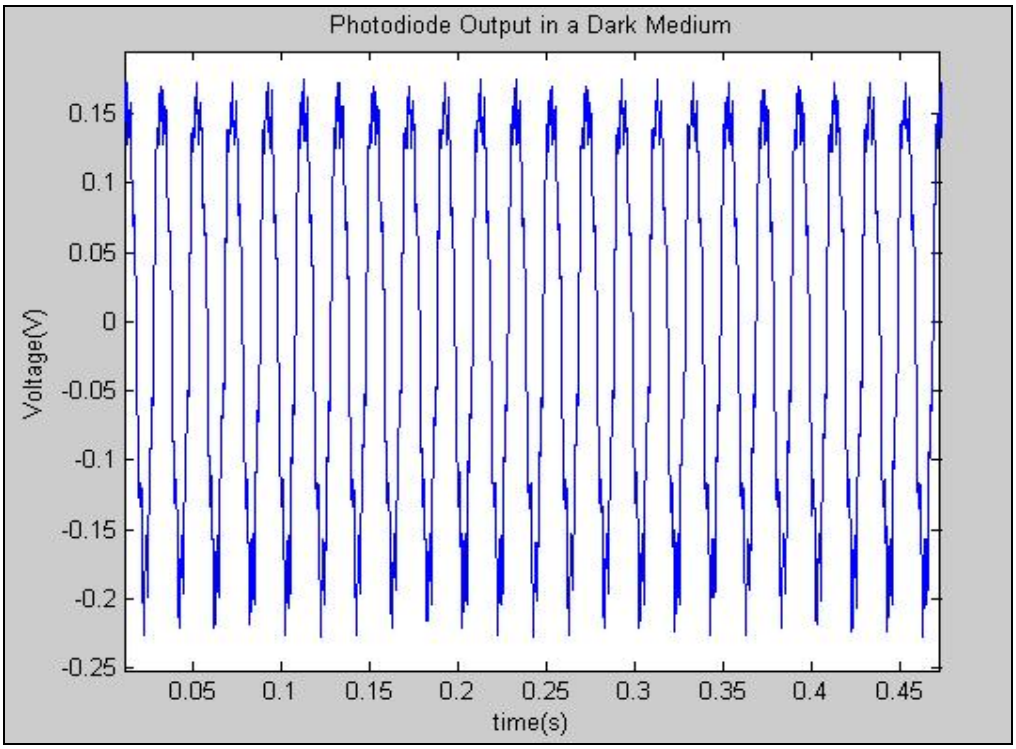

Figure 4.1 Raw photodiode output in a dark medium.

4.1.2 Output of the Amplifier and Filter in a Dark Medium

Figure 4.2 depicts the output of the circuit when the photodiode is put in a dark medium. A lower 50 Hz noise is also seen at the output, this actually stems from the daqcard connection which also gets noise. There are also undesired spikes seen in the figure which are invisible on the oscilloscope screen. This is also resulted from the connection between the output of the circuit and the daqcard. The standart deviation of the signal is 0.0086, the mean value and variance are 0.0546 and 7.3×10^{-5}, respectively.

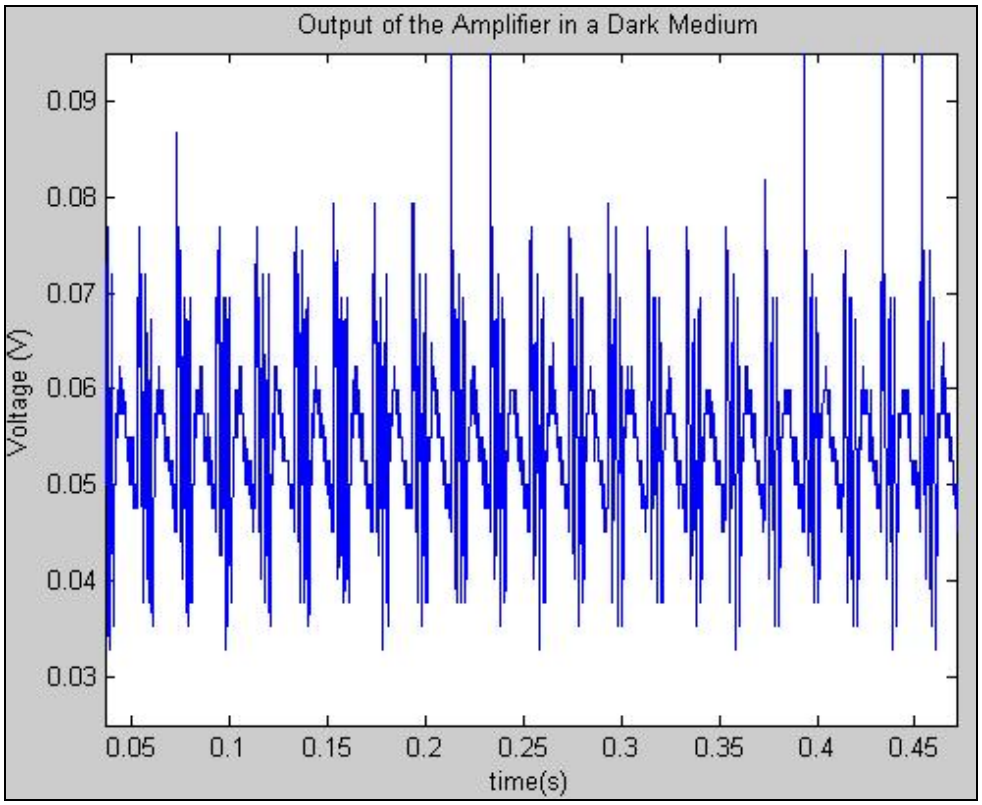

Figure 4.2 Output signal in a dark medium when no laser is running.

4.1.3 Temperature Dependency of the Lasers

Laser drivers can shutdown the lasers in an overcurrent or overtemperature situation to protect the lasers. Since lasers were driven in a continuous mode, cooling system was needed.

In order to see the change of temperature in the case with respect to temperature outside, the unit was inserted in a box whose one side is open. Then, the probe of the data logger (Hanna Instruments) was inserted inside the unit and and external digital thermometer was put outside of the case. From the open side of the box, the heater was run until the external thermometer indicated about 40 ^{0}C (26th minute) while the data logger inside was showing 31.9 ^{0}C. Then the heater was closed for the unit to cool down. In Figure 4.3, all the readings recorded for forty minutes were shown.

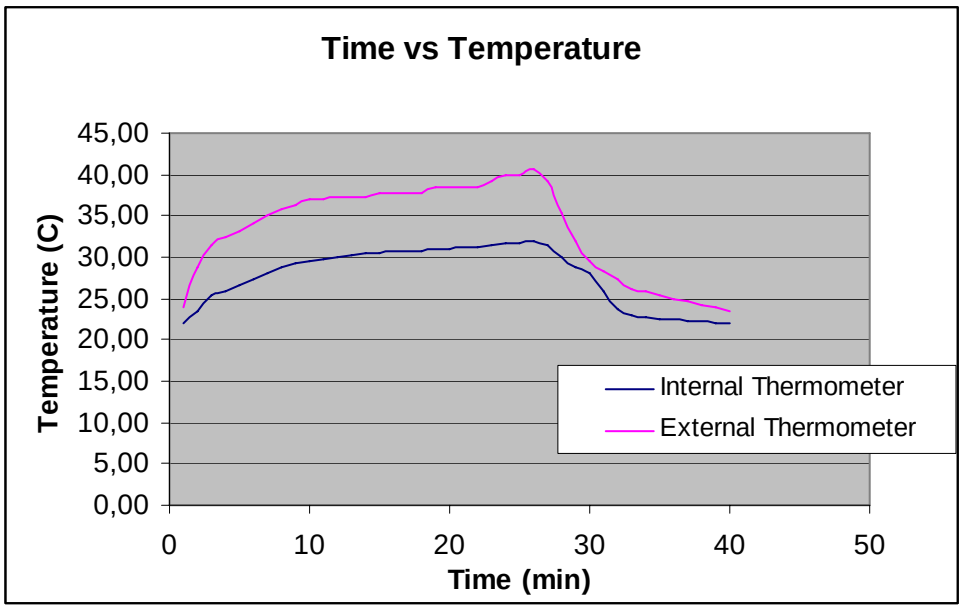

Figure 4.3 External and internal thermometer readings while changing temperature

To test the output change with temperature, the setup in Figure 4.4 was constructed on a phantom.

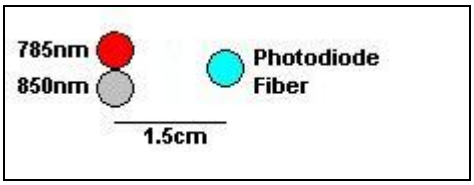

Figure 4.4 The setup to measure the outputs of lasers.

The 785 nm laser modulated with 1 kHz and the 850 nm laser modulated with 360 Hz were run at the same time. The probe of the data logger was inserted inside the case and it was waited for several minutes to reach the coolest degree by just running the cooling air fans. Then 23.2 ^{0}C was read on the data logger and the temperature was changed by 2.5 ^{0}C

increments by hair dryer. At each value of temperature, a four minute measurement was performed and mean values were calculated. In Figure 4.5, the output voltages of both 850 nm and 785 nm diode lasers with respect to temperature were seen. It is noted that after 30 ^{0}C internal temperature, the output voltages decreased slightly.

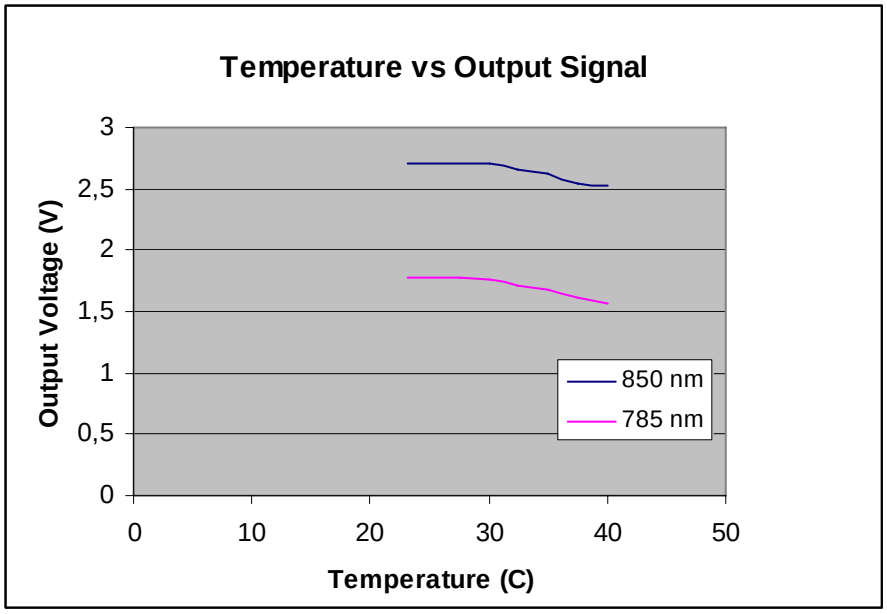

Figure 4.5 Output signals of both lasers with respect to temperature

The mean and peak values are not so important for this measurement because they can be brought to same levels by changing the adjustable resistors of the monitor photodiodes and amplitude of the sine wave generators.

4.1.4 Change of Output Power with Different Laser Detector Distances

The weakness of the system is that the output signal drops rapidly as the distance increases. To study the hemodynamic response in the brain the detector laser distance should be approximately 2.5 cm. The current lasers are suitable for the measurement at maximum 1.5 cm distance (Figure 4.6).

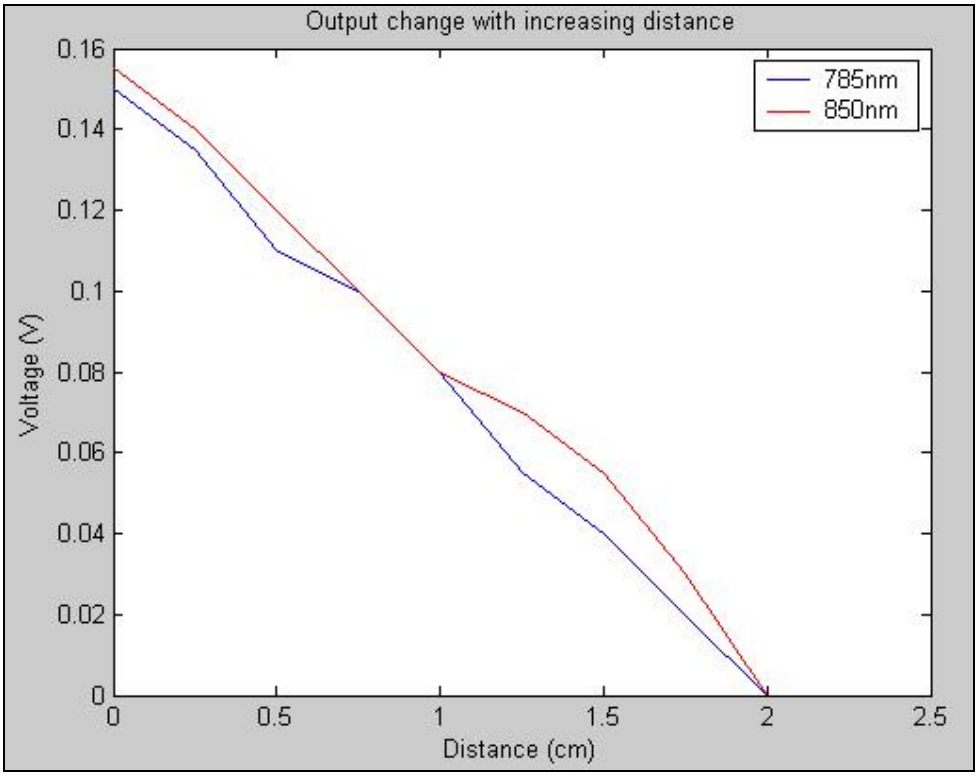

Figure 4.6 Output signal change with distance.

4.2 Experimental Studies

Two studies were done for the experimental verification. Ischemia was performed in human and rat to see the oxyhemoglobin (HBO_2) and deoxyhemoglobin (HB) concentration changes. These were done successfully.

4.2.1 Ischemia Performed in Human

The fibers from the lasers and photodiode fiber were placed to the subject arms projected on the extensor carpi as in Figure 4.3. The first sixty seconds, it is just waited motionless to form a baseline. Then cuff was inflated to block the blood flow and waited for two minutes and finally it is waited for one minute to see the recovery period.

In Figures 4.7 and 4.8, concentration changes of Hb and HbO_2 were shown. These changes were calculated using the Eq. 2.11 and Eq. 2.12. As it is seen, after the sixty

seconds, while there is an increase in Hb level, HbO_2 level is decreasing at the end of the two minutes ischemia. The recovery period is seen after the a hundred and eighty seconds.

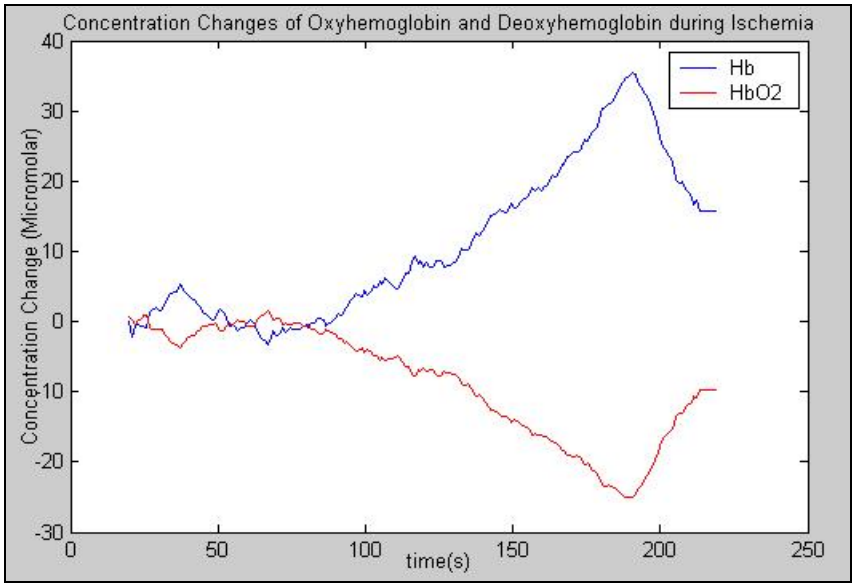

Figure 4.7 Concentration changes of Hb and HbO_2 during ischemia in subject 1.

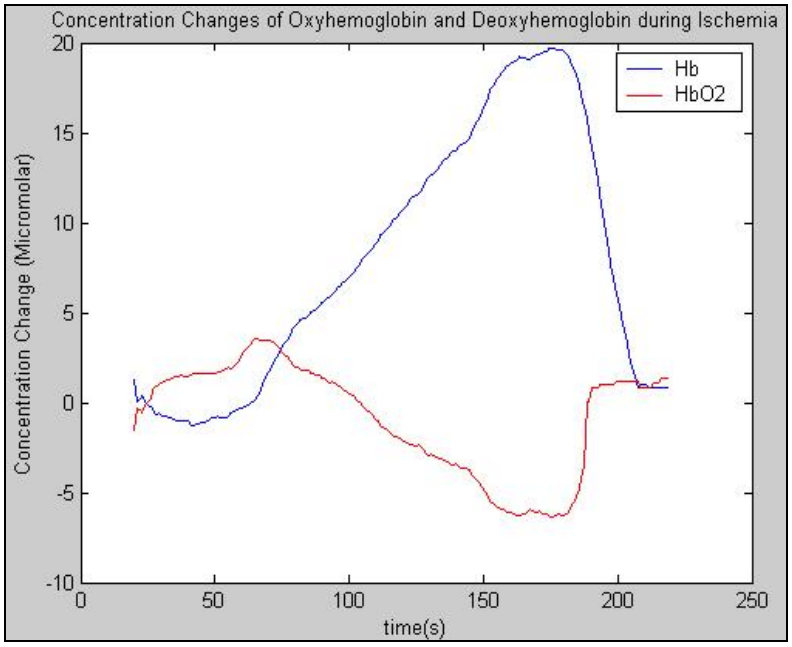

Figure 4.8 Concentration change od Hb and HbO2 during ischemia in subject 2.

To check that all four channels operate properly, the fibers were placed on the muscle as in Figure 4.9.

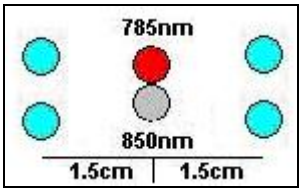

Figure 4.9 The setup to check the channels.

The results from the four channels were seen in Figure 4.10. It is apparently seen that ΔHb increases during the ischemia, whereas ΔHbO_2 decreases. At sixtieth second, the Hb and HbO_2 concentration begins to change as expected. At the end of three minutes, again they begin to go to their initial conditions.

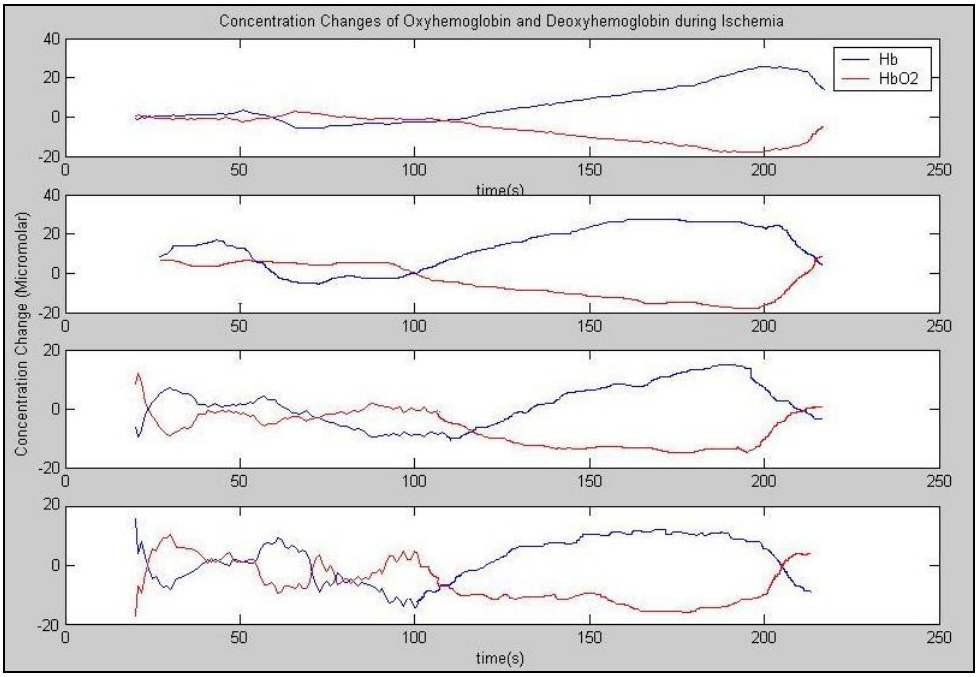

Figure 4.10 Concentration changes of Hb and HbO_2 during ischemia in four channels.

4.2.2 Ischemia Performed in a Rat

A male rat weighted 415 gr was used in the experiment. Total 4.98 ml anesthesia was given. The first half was given and it is waited for ten minutes then the remaining part was given. The temperature of the rat was fixed at 37 ^{0}C with the microprocessor controlled heated pad.

The optical fibers were placed in the middle of the tibialis anterior muscle as shown in Figure 4.11. The distance between the sources (lasers) and detector is 1.5 cm. The data was acquired in four minutes and in five minutes sets. In the former, sixty seconds formed the baseline then the ischemia was done in two minutes by tightening the tourniquet and the recovery was waited for one minute. The latter was done to see the recovery period better. forty seconds formed the baseline and ischemia was performed for two minutes then the tourniquet was untightened and waited to see going back of the signals to the baseline.

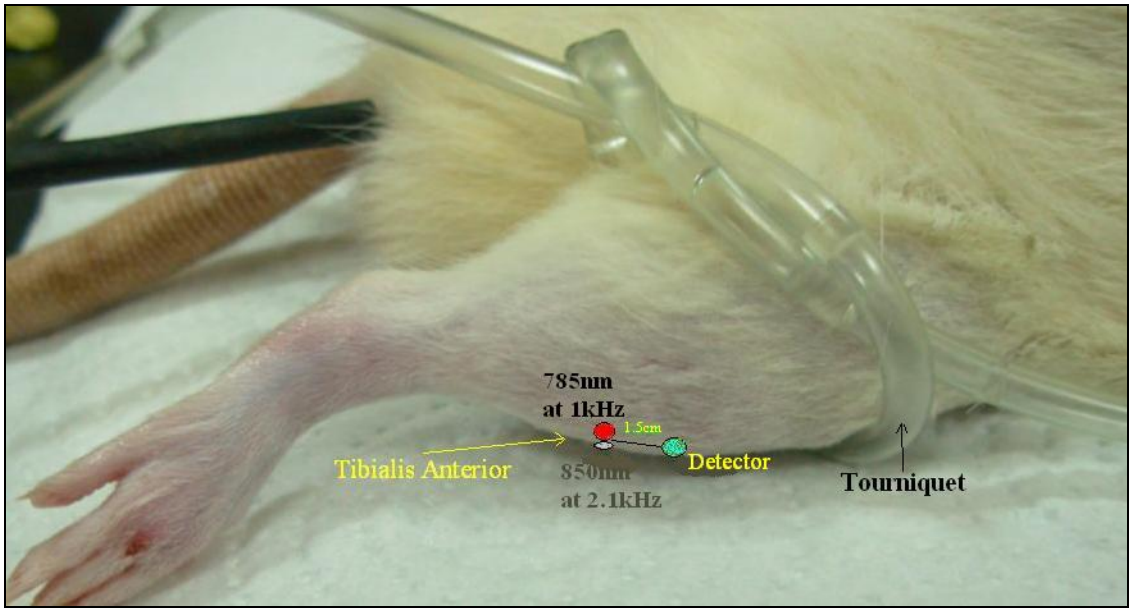

Figure 4.11 Fiber cables in the middle of the tibialis anterior muscle.

The recovery period is seen better from Figure 4.12 and 4.13. After the 40 seconds, the expected change happened and two minutes later the Hb level went down and HbO_2 went up to their initial conditions as expected. However, they did not intersect each other. This can be resulted from that they need more time to go back to the baseline.

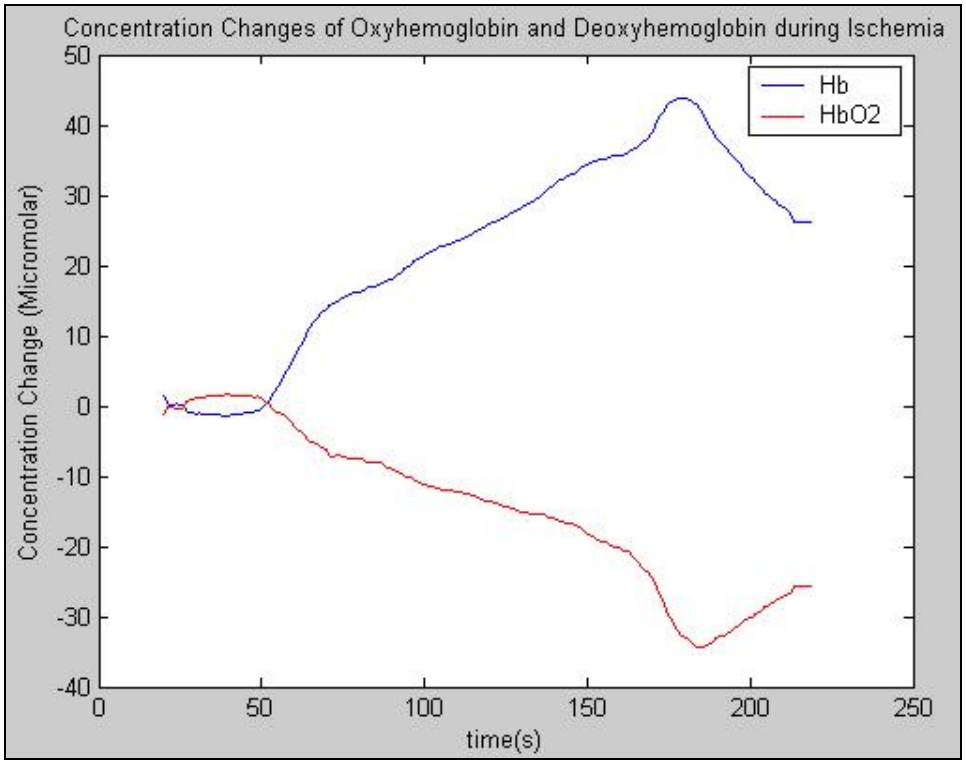

Figure 4.12 Hb and HbO_2 concentration change with ischemia in a rat in four minutes.

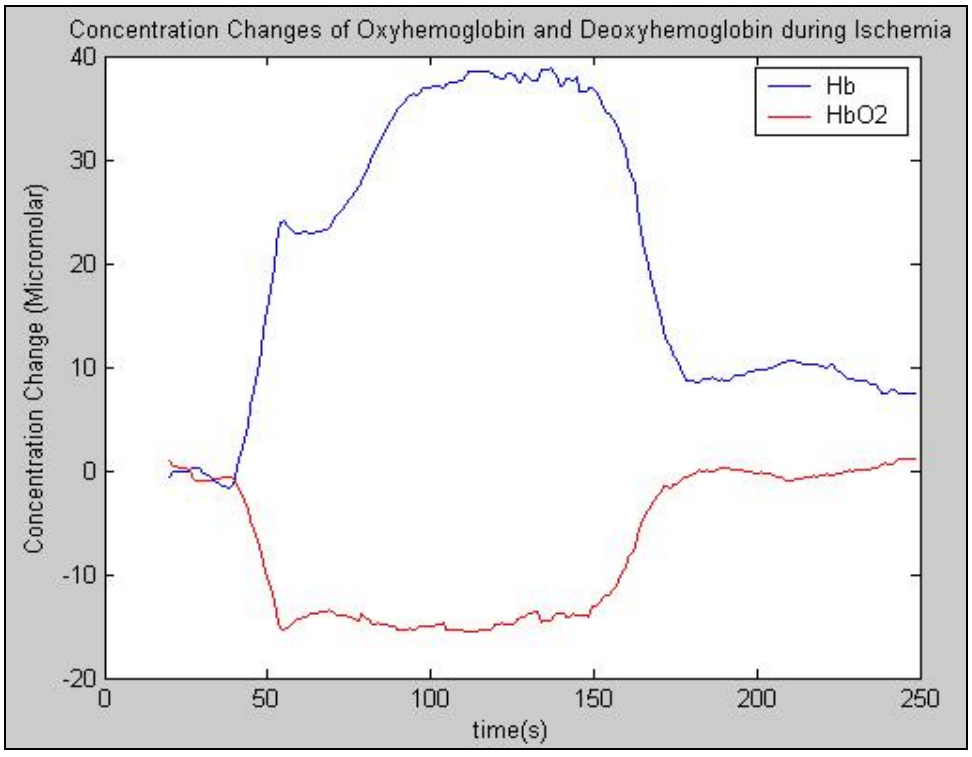

Figure 4.13 Hb and HbO_2 concentration change with ishemia in a rat in five minutes.

5. CONCLUSIONS AND FUTURE WORK

In this thesis, design and implementation of a fiber optic based continuous wave near infrared spectroscopy system are presented. The system works successfully up to a source-detector distance of one and a half centimetre which can be useful to investigate the hemodynamic changes in a muscle activity. It is also useful for animal imaging which does not require long source detector distances with miniaturized source and detectors. However, intended two and a half centimetre source-detector distance could not be achieved and hence the system is not suitable to study the cortical hemodynamic changes.

One of the most challenging parts of the work was to drive the lasers successfully. This was dealt with IC-Haus drivers having the protection shutdown switches and enabling the output power modulation without requiring any external components. Fiber coupling was another important point in the design and was successfully overcome by the thorlabs optical focusing tubes and lens. However, the fibers (3mm core diameter) available in the market were not highly appropriate for the power transmission of lasers having such wavelengths. Additionally, it was a difficult task to fix the fibers on the measurement place because of its inflexibility. Furthermore, air fans were used to cope with the heating problem successfully. Even if both lasers were continuously run twenty minutes, no drop in the output voltage level was observed.

Sampling rate of the data acquisition card was very crucial to convert the analog signal to digital for further processing and analyzing. NI daqcard in the biomedical optics laboratory has a very high sampling rate and therefore very successful in digitizing the modulated signals. However, the trouble with the daqcard was its noisy input since it was not located in an isolated case. Although the noise from the power line was almost suppressed completely (seen on the oscilloscope screen), it appears again in the input of the daqcard. On the other hand, this inevitable noise was filtered out by the signal processing techniques to get a smooth data.

To investigate the cortical hemodynamics that lie underneath places covered with hair, coupling fibers to the light sources is inevitable. Therefore, using laser diodes instead of LEDs is an obligatory task. However, because of difficulties in coupling and high

transmission loss in poor quality fibers, it is better to use fiber-pigtailed lasers which will transmit the desired power directly to the distal end of the fiber. Otherwise, more powerful lasers should be used to get the scattered light from two and a half centimeter distance. Furthermore, detector amplifiers and filters can also be improved using high quality opamps and constructing more advanced circuits. Including the band pass filters in the circuitry will lighten the workload of the processing unit.

APPENDIX A. SCHEMATIC

The schematic of the transmitter and receiver units were drawn by OrCad 9.1 Capture program.

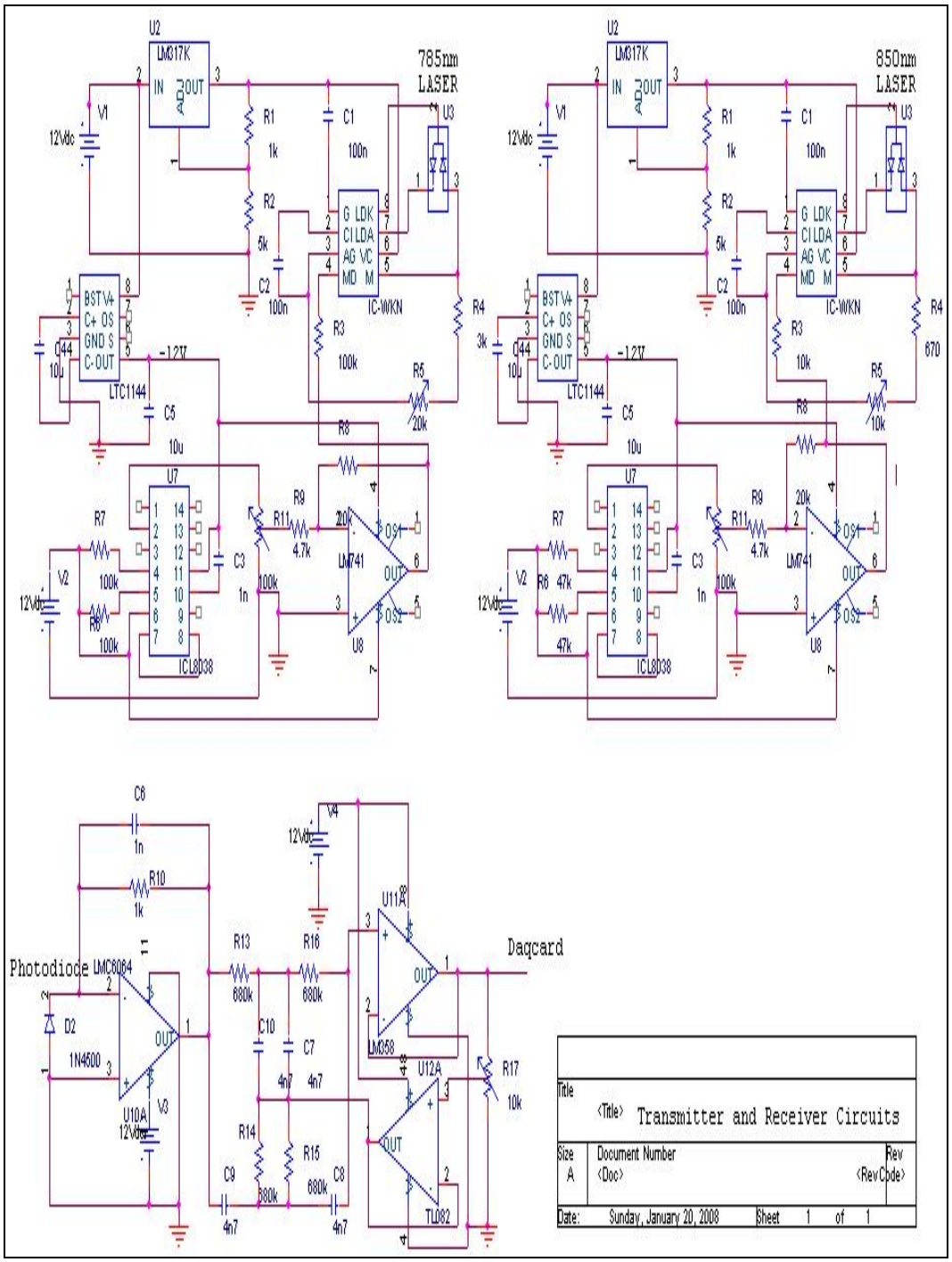

Figure A.1 Schematic of transmitter and receiver units

APPENDIX B. MATLAB CODES

B.1 Matlab Code to Acquire and Analyze Data from National Instrument Hardware

```
% Use this command to determine Board IDs in system, if needed
hw = daqhwinfo('nidaq')
hw.InstalledBoardIds
hw.BoardNames

% Create an analog input object using Board ID "Dev6".
ai = analoginput('nidaq','1');

% Data will be acquired from hardware channel 0-3
addchannel(ai, 0:3);

% Review the basic configuration of the acquisition by typing
% the name of the variable.

% ai

% Use this command to see properties that can be configured
% set(ai)

% Use this comment to get a listing of all object properties and
% their current settings
% get(ai)

% Configure the analog input for single-ended or differential mode

set(ai,'InputType','SingleEnded');
% set(ai,'InputType','Differential');

% Set the sample rate and samples per trigger
samplerate=10000
```

```
set(ai,'SampleRate', samplerate)
ActualRate = get(ai,'SampleRate')
totalduration=ActualRate*240
set(ai,'SamplesPerTrigger',totalduration)

% Start the acquisition
start(ai);

% Wait up to 2 seconds for the acquisition to complete
%waittilstop(ai,2);

% Acquire data into the MATLAB workspace
data = getdata(ai);

% Clean up
stop(ai);
delete(ai);
```

B2. Matlab Code to Separate the Modulated Signals and for Envelope Detector

```
t=(1:length(data(:,1)))*(1/10000);

%Band pass filter 1 kHz
 [b,a] = butter(4,[800 1200]/(samplerate/2));

%Envelope detector
data785=filtfilt(b,a,data(:,1));
fort2=data785.^2;
[b1,a1]=butter(4,1000/5000);
fort2f=filtfilt(b1,a1,fort2);
fort2fr=resample(fort2f,1,10);
tr=resample(t,1,10);
[b1,a1]=butter(4,100/500);
fort2f=filtfilt(b1,a1,fort2fr);
```

```
fort2fr=resample(fort2f,1,10);
tr=resample(tr,1,10);
[b1,a1]=butter(4,10/50);
fort2f=filtfilt(b1,a1,fort2fr);
fort2fr=resample(fort2f,1,10);
tr=resample(tr,1,10);
[b1,a1]=butter(4,1/5);
fort2f=filtfilt(b1,a1,fort2fr);
fort2fr=resample(fort2f,1,10);
tr=resample(tr,1,10);
fort2fr785=fort2fr;

%Removing the beginning and end of the signals
m=find(tr<20);
m1=max(m);
m=find(tr<220);
m2=max(m);
L=length(tr);
trm=tr(m1:m2);
fort2frm785=fort2fr785(m1:m2);

%Band pass filter 360 Hz
 [b,a] = butter(4,[100 600]/(samplerate/2));

%Envelope Detector
data850=filtfilt(b,a,data(:,1));
fort2=data850.^2;
[b1,a1]=butter(4,1000/5000);
fort2f=filtfilt(b1,a1,fort2);
fort2fr=resample(fort2f,1,10);
tr=resample(t,1,10);
[b1,a1]=butter(4,100/500);
fort2f=filtfilt(b1,a1,fort2fr);
fort2fr=resample(fort2f,1,10);
tr=resample(tr,1,10);
[b1,a1]=butter(4,10/50);
```

```
fort2f=filtfilt(b1,a1,fort2fr);
fort2fr=resample(fort2f,1,10);
tr=resample(tr,1,10);
[b1,a1]=butter(1,1/5);
fort2f=filtfilt(b1,a1,fort2fr);
fort2fr=resample(fort2f,1,10);
tr=resample(tr,1,10);
fort2fr850=fort2fr;
m=find(tr<20);
m1=max(m);
m=find(tr<220);
m2=max(m);
L=length(tr);
trm=tr(m1:m2);
fort2frm850=fort2fr850(m1:m2);
```

B3. Matlab Code to Plot Concentration Changes of Oxy and Deoxyhemoglobin

```
%Calculating the absorbance of 785nm laser
output785 = tsmovavg(fort2frm785', 's',7,7);
od785=log(mean(output785(1:10))./output785);



%Calculating the absorbance of 850nm laser
output850 = tsmovavg(fort2frm850', 's',7,7);
od850=log(mean(output850(1:10))./output850);

%Calculating the concentrations of Hb and HbO2
dpf_degeri=6
d = 1.5; % [cm]
d_carpi_DPF = d*dpf_degeri % d * DPF [cm], d=2.5 cm
        eHB_785= 9.97e-5*10; % micro M cm -1
        eHB_850= 0.0000786*10;
```

```
        eHBO2_785= 7.67e-5*10;
        eHBO2_850= 0.0001159*10;
HB=(od785*eHBO2_850-od850*eHBO2_785)/(eHBO2_850*eHB_785-
eHBO2_785*eHB_850)/d_carpi_DPF;
HBO2=(od785*eHB_850-od850*eHB_785)/(eHBO2_785*eHB_850-
eHBO2_850*eHB_785)/d_carpi_DPF;

%Graphically plot the results
plot(trm,HB,trm,HBO2, 'r')
xlabel('time(s)');
title('Concentration Changes of Oxyhemoglobin and Deoxyhemoglobin during Ischemia');
ylabel('Concentration Change (Micromolar)');
legend('Hb', 'HbO2')
```

APPENDIX C. DATA SHEETS

This section includes the data sheets of laser diodes and photodiodes used in the system.

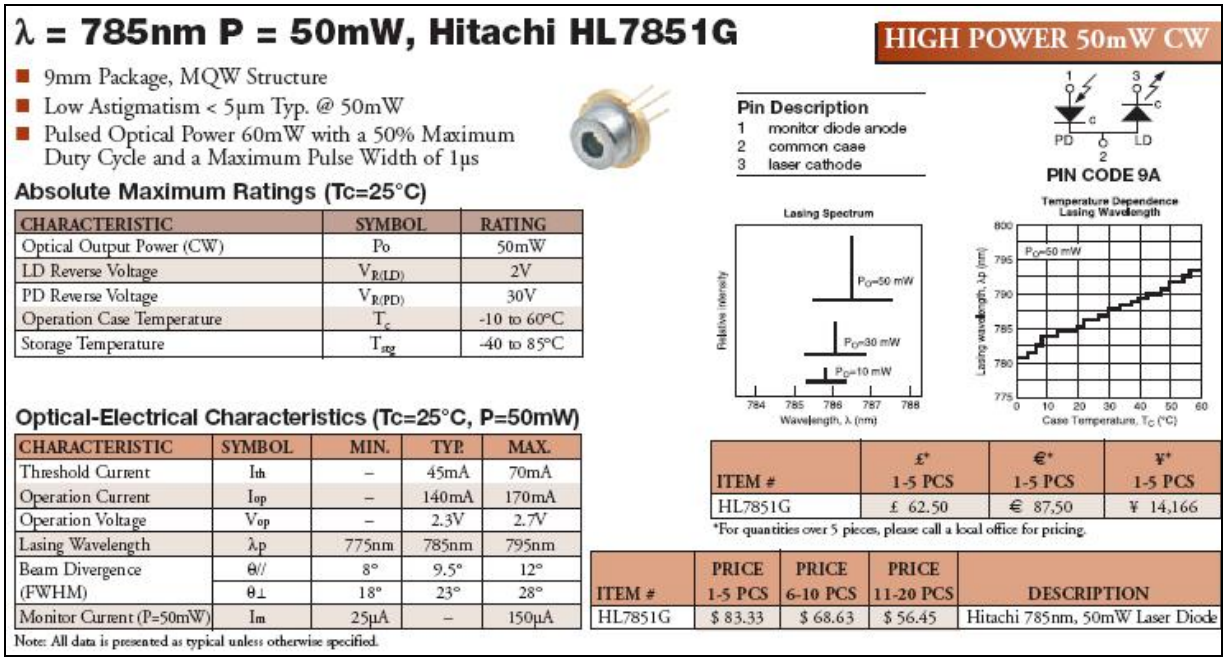

λ = 785nm P = 50mW, Hitachi HL7851G

HIGH POWER 50mW CW

- 9mm Package, MQW Structure
- Low Astigmatism < 5μm Typ. @ 50mW
- Pulsed Optical Power 60mW with a 50% Maximum Duty Cycle and a Maximum Pulse Width of 1μs

Pin Description
1 monitor diode anode
2 common case
3 laser cathode

PIN CODE 9A

Absolute Maximum Ratings (Tc=25°C)

CHARACTERISTIC	SYMBOL	RATING
Optical Output Power (CW)	Po	50mW
LD Reverse Voltage	$V_{R(LD)}$	2V
PD Reverse Voltage	$V_{R(PD)}$	30V
Operation Case Temperature	T_c	-10 to 60°C
Storage Temperature	T_{stg}	-40 to 85°C

Lasing Spectrum

Temperature Dependence Lasing Wavelength

Optical-Electrical Characteristics (Tc=25°C, P=50mW)

CHARACTERISTIC	SYMBOL	MIN.	TYP.	MAX.
Threshold Current	Ith	–	45mA	70mA
Operation Current	Iop	–	140mA	170mA
Operation Voltage	Vop	–	2.3V	2.7V
Lasing Wavelength	λp	775nm	785nm	795nm
Beam Divergence (FWHM)	θ//	8°	9.5°	12°
	θ⊥	18°	23°	28°
Monitor Current (P=50mW)	Im	25μA	–	150μA

Note: All data is presented as typical unless otherwise specified.

ITEM #	£* 1-5 PCS	€* 1-5 PCS	¥* 1-5 PCS
HL7851G	£ 62.50	€ 87,50	¥ 14,166

*For quantities over 5 pieces, please call a local office for pricing.

ITEM #	PRICE 1-5 PCS	PRICE 6-10 PCS	PRICE 11-20 PCS	DESCRIPTION
HL7851G	$ 83.33	$ 68.63	$ 56.45	Hitachi 785nm, 50mW Laser Diode

Figure C.1 Data sheet of 785nm laser.

THORLABS INC
435 Route 206 • P.O. Box 366
Newton, NJ 07860-0366

SALES 973-579-7227
FAX 973-300-3600

Laser Diode Technical Data

L850P100

Features

- Index Guided MQW Structure
- Wavelength : 850 nm (Typ.)
- Optical Power : 100 mW CW
- Threshold Current : 70 mA (Typ.)
- Package Style : TO-18 (5.6 mmØ)

ABSOLUTE MAXIMUM RATINGS (Tc=25 °C)

DESCRIPTION	SYMBOL	RATED VALUE
Optical Power (mW)	P_o	100
Operation Temperature (°C)	T_{op}	-10 to +50
Storage Temperature (°C)	T_{stg}	-40 to +85
LD Reverse Voltage (V)	V_{LDR}	2
PD Reverse Voltage (V)	V_{PDR}	30

OPTICAL AND ELECTRICAL CHARACTERISTICS (Tc=25 °C)

DESCRIPTION	SYMBOL	MIN.	TYPICAL	MAX.	TEST CONDITION
Lasing Wavelength (nm)	λ_p	835	850	865	P_o=100mW
Threshold Current (mA)	I_{th}	50	70	90	P_o=100mW
Operating Current (mA)	I_{op}	150	200	350	P_o=100mW
Operating Voltage (V)	V_{op}	1.8	2.0	2.5	P_o=100mW
Monitor Current (mA)	I_m	0.1	0.3	1.5	P_o=100mW, V_R=5V
Slope Efficiency (mW/mA)	η	0.5	0.7	0.9	***
Beam Divergence ∥ (°)	$\theta\parallel$	8	10	12	P_o=100mW
Beam Divergence ⊥ (°)	$\theta\perp$	25	30	40	P_o=100mW
Astigmatism (μm)	A_s	*	11	*	P_o=100mW,NA=0.4

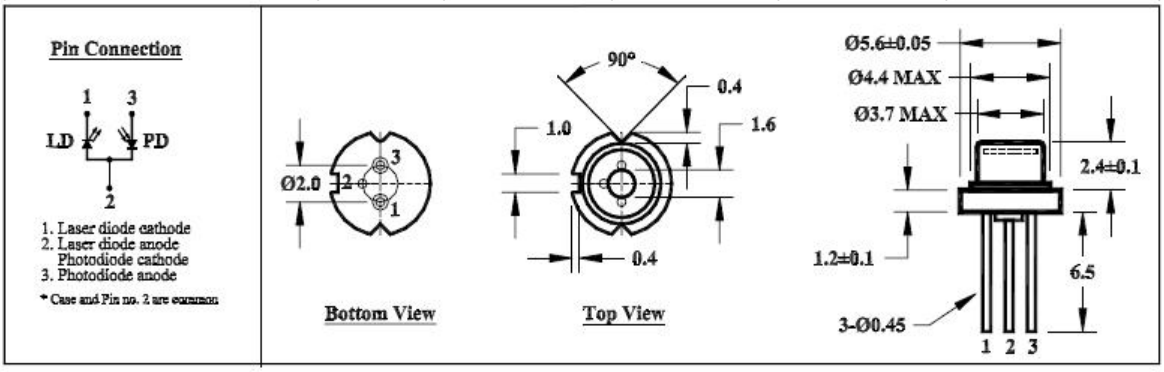

Figure C.2 Data sheet of the 850nm laser.

THORLABS INC
435 Route 206 • P.O. Box 366
Newton, NJ 07860-0366
Phone: 973-579-7227
FAX: 973-300-3600

SM05PD1A Mounted Silicon-Photodiode

High Speed
Large Active Area

The SM05PD1A is a high-speed mounted silicon photodiode with a spectral response from 350nm to 1100nm. This photodiode has a PIN structure that provides fast Rise/Fall Times (20ns) with a bias of 12V. The SM05PD1A is compatible with all Thorlabs SM05 Mounting components.

Electrical Characteristics:

Spectral Response:	350 - 1100nm
Active Area:	13.0mm²
Rise Time (R_L = 50Ω):	20ns (12V bias)
Fall Time (R_L = 50Ω):	20ns (12V bias)
NEP @900nm:	1.2×10^{-14} W/√Hz (@12V bias)
Dark Current:	20nA max. (12V)

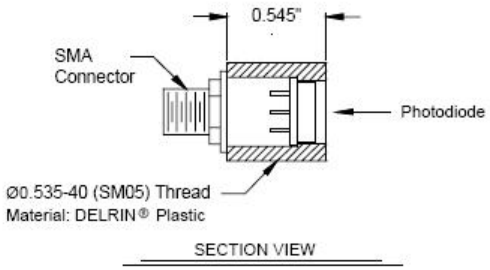

SECTION VIEW

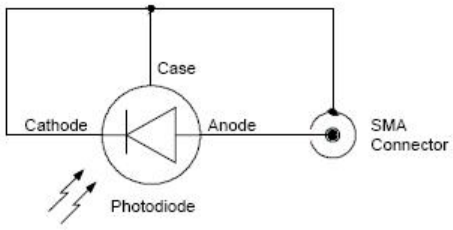

ELECTRICAL CONNECTION

Maximum Ratings:

Damage Threshold CW:	100mW/cm²
Damage 10ns Pulse:	500mJ/cm²
Max Bias Voltage:	25V

The Thorlabs SM05PD1A Mounted Silicon-Photodiode is ideal for measuring both pulsed and CW light sources, by absorption of photons or charged particles and generate a flow of current in an external circuit, proportional to the incident power. The photodiode anode produces a current, which is a function of the incident light power (P) and the wavelength (λ). The responsivity R_λ, can be read from Fig.1 to estimate the amount of photocurrent to expect. This can be converted to a voltage by placing a load resistor (R_L) from the photodiode anode to the circuit ground. The output voltage is derived as:

$$V_0 = P \cdot R_\lambda \cdot R_L$$

The bandwidth (f_{BW}) and the rise time response (t_R), are determined from the diode capacitance (C_J) and the load resistance (R_L) as shown below. Placing a bias voltage from the photo diode cathode to the circuit ground can lower the photo diode capacitance.

$$f_{BW} = \frac{1}{2\pi \cdot R_L \cdot C_J} \qquad t_R \cong \frac{0.35}{f_{BW}}$$

Figure C.3 Data sheet of the photodiode.

APPENDIX D. USER MANUAL

This section provides information on the functions of the unit. It contains important safety and operation information.

D1. The Unit Overview

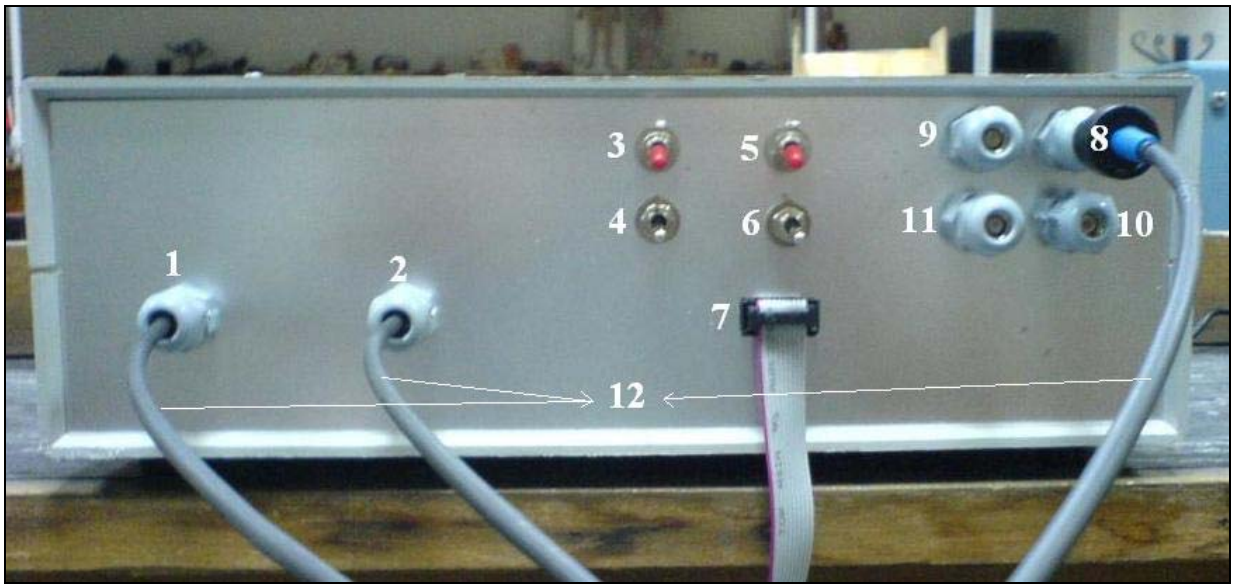

Figure D.1 Front view of the unit.

1. 785 nm laser output.
2. 850 nm laser output.
3. 785 nm laser ON(up)/OFF(down) button.
4. 785 nm laser modulation ON(up)/OFF(down) button.
5. 850 nm laser ON(up)/OFF(down) button.
6. 850 nm laser ON(up)/OFF(down) button.
7. Output to PC daqcard.
8. Input channel 1.
9. Input channel 2.
10. Input channel 3.
11. Input channel 4.
12. Optical fibers.

Figure D.2 Back view of the unit.

13. Power input.
14. Power switch.
15. Cooling fans.

D2. Operation

1. Please be sure that the power supply cable is connected to the power input (13 in Figure D.2) at the rear of the case.
2. Turn the power switch (14 in Figure D.1) to “I” position and check that the air fans are operating.
3. First of all, turn the laser power switches (3, 5 in Figure D.1) on. Then, turn on the modulation switches (4, 6 in Figure D.1) which modulate the output powers of 785nm and 850nm lasers by 1 kHz and 360 Hz, respectively.
4. Open the Matlab 6.5 tool and fiberbasednirs.m file on the PC. Then specify the data acquisition duration in seconds as it is stated 240s in Appendix B and section heading B.2 in line;

totalduration=ActualRate*240

Note that exceeding the 300s could result in run time error.

5. After the measurements are taken, turn off firstly the modulation switches (4, 6 in Figure D.1) and then the laser power switches (3, 5 in Figure D.1)
6. Then wait for two minutes at least to allow the air fans to cool the laser diodes sufficiently.
7. Finally, turn the power switch (14 in Figure D.2) to "0" position to turn off the air fans as well.

D3. Cautions

To turn on the modulation switches (4, 6) prior to laser power switches could result in burning out the laser diodes. Therefore, please turn the laser power switches (3, 5) on first and then turn the modulation switches (4, 6) on.

Before switching off the device (the powers and modulations (3, 4, 5, 6) are already in off positions), please allow the air fans to run at least two minutes for enough cooling of the laser diodes. Otherwise, they can be burnt out.

Class IIIb Laser Products.
AVOID EYE EXPOSURE TO DIRECT OR SCATTERED RADIATION.

REFERENCES

1. Sergio Fantini et al., Monitoring brain activity using near-infrared light, *American Laboratory*, October 2001.

2. Izzetoglu, K., Bunce, S., Izzetoglu, M., Onaral, B., and K. Pourrezaei, "Functional Near-infrared Neuroimaging," in the *Proceedings of the 26th Annual International Conference of the IEEE EMBS*, San Francisco, CA, 2004.

3. Elwell, C., and J. Hebden, "Near – Infrared Spectroscopy," January 1999. Available: www.medphys.ucl.ac.uk.

4. Aslin R.N., and J. Mehler, "Near-infrared spectrsocopy for functional studies of brain activity in human infants, promise, prospects and challeges," *Journal of Biomedical Optics*, Vol. 10(1), February 2005.

5. Jöbsis, F. F., "Non invasive, infrared monitoring of cerebral and myocardial oxygen suficency and circulatory parameters," *Science*, Vol. 198, pp. 1264 – 7, 1997.

6. Okada, E., M. Firbank, M. Schweiger, S. R. Arridge, and M. Cope, "Theoretical and experimental investigation of near-infrared light propagation in a model of the adult head," *Applied Optics*, Vol. 36, pp. 21-31, 1997.

7. Stepnoski , R. A., LaPorta, A., Raccuia-Behling, F., Blonder, G.E., Slusher, R.E., D. Kleinfeld, "Noninvasive detection of changes in membrane potential in cultured neurons by light scattering," *Proceedings of the National Academy of Science,* Vol. 88, pp. 9382-6, 1991.

8. Haensse, D., P. Szabo et al., "New multichannel spectrophotometry system for functional studies of the brain in adults and neonates," *Optics Express,* Vol. 13, No. 12, June 2005.

9. Gratton, G. and M. Fabiani, "Shedding light on brain function: the eventrelated optical signal," *Trends in Cognitive Science,* Vol. 5, pp. 357-363, 2001.

10. Medicins Sons Frontieres, *In-Vivo Analysis Techniques*, 2007, Available: http://focosi.immunesig.org/invivo.html.

11. Paunescu, L. A., *Tissue blood flow and oxygen consumption measured with near-infrared frequency-domain spectroscopy*. PhD thesis, University of Illinois, Urbana-Champaign, 2001.

12. Tuchin, V., Tissue Optics, Spie Press, Washington, USA, 2000.

13. Emir, U., "System characterization for a fast optical imager," Master's thesis, Bogazici University , Istanbul, Turkey, 2003

14. Boas et al., "Imaging the body with diffuse optical tomography," *IEEE Signal Processing Magazine*, 2001.

15. Cheong, W., Prahl, S.A., and A. J. Welch, "A review of the optical properties of biological properties," *IEEE Journal of Quantum Electronics*, Vol. 26, pp. 2166-85, Dec 1990.

16. Duncan, A., J. H. Meek, M. Clemence, C. E. Elwell, L. Tyszczuk, Cope, M., and D. T. Delpy, "Optical pathlength measurements on adult head, calf and forearm and the head of the newborn

infant using phase resolved optical spectroscopy," *Physics in Medicine and Biology* Vol. 40, pp. 295-304, 1995.

17. Patterson, M. S., Chance, B., and B. C. Wilson (1989). "Time resolved reflectance and transmittance for the non-invasive measurement of tissue optical properties," *Applied Optic,* Vol. 28, pp. 2331-2336, 1989.

18. Chance, B., M. Cope, E. Gratton, Ramanujam, N., and B. Tromberg, "Phase measurement of light absorption and scatter in human tissue," *Review of Scientific Instruments* Vol. 69**,** pp. 3457-3481, 1998.

19. Force Incorporated, *Laser Diodes*, 2005, http://www.fiber-optics.info/articles/laser-diode.htm.

20. Malzahn, U. M., "Driving laser diodes," *Europhotonics*, Vol. 8, pp. 22-23, 2004.

21. Malzahn, U. M., *Operating sanyo laser diodes with integrated drivers*, *Notes of IC-Haus Integrated Circuits Company,* 2006.

22. National Instruments, "DaqE series user Manual," pp. A99-101, Feb 2007.